This is a preprint, the final version is subject to change, of the American Mineralogist (MSA)
Cite as Authors (Year) Title. American Mineralogist, in press.
(DOI will not work until issue is live.) DOI: http://dx.doi.org/10.2138/am-2016-5521

From phosphates to silicates and back – an experimental study on the transport and storage of phosphorus in eclogites during uplift and exhumation

Jürgen Konzett

Institute of Mineralogy and Petrology, University of Innsbruck, Innrain 52, A-6020 Innsbruck, Austria

e-mail: juergen.konzett@uibk.ac.at

revision 2

This is a preprint, the final version is subject to change, of the American Mineralogist (MSA)
Cite as Authors (Year) Title. American Mineralogist, in press.
(DOI will not work until issue is live.) DOI: http://dx.doi.org/10.2138/am-2016-5521

ABSTRACT

High-*P*-*T* experiments have shown that in major rock types such as MORBs, peridotites and pelitic sediments, increasing *P* (and *T*) leads to a gradual transfer of P from phosphates mostly represented by apatite to silicates with garnet as most important silicate P carrier. This is due to the formation of a $Na_3Al_2(PO_4)_3$ phase component in garnet via $^{[8]}Na^{[4]}P^{[8]}M^{2+}{}_{-1}{}^{[4]}Si_{-1}$ which is strongly *P*-, and to a lesser extent *T*-dependent and creates garnets with significant P and Na at *P* as low as 2-3 GPa. Based on this experimental evidence one would expect to routinely find P-Na-rich garnets in UH*P*-rocks with a wide range in composition. With very few exceptions, however, this is not the case. This discrepancy indicates that both P and Na are effectively released from garnet and re-distributed within the garnet matrix during uplift and exhumation. In order to explore the mechanisms of this P-Na release, P-Na-rich garnet pre-synthesized at 7 GPa and 1200°C, containing 0.7 wt% P_2O_5 and 0.3 wt% Na_2O, was exposed to *P*-*T* conditions of 2 GPa and 800-1000°C in a simplified, H_2O-bearing, model eclogitic bulk composition. The experiments show that at subsolidus temperatures of 850-975°C, and in the presence of a hydrous fluid, apatite quickly forms from garnet breakdown involving consumption of coexisting quartz and clinopyroxene. The apatites usually appear as rounded to lath-shaped isolated grains scattered in the garnet + clinopyroxene ± orthopyroxene + quartz + rutile matrix. More rarely, single apatite inclusions, or clusters of inclusions, may form in clinopyoxene or garnet. The observed apatite grain size is in the range ≤ ~1x1 to 24x6 µm with the largest grains occasionally containing clinopyroxene inclusions. Combined garnet breakdown and neo-formation, using pre-existing garnet as a nucleation site, may form zoned garnets with Na-P depleted and Ti-enriched rims that represent an approach to a garnet composition typical for mid- to shallow crustal *P*-*T* conditions. Partial melting experiments indicate that eclogites containing P-rich garnet may produce P-rich and apatite-undersaturated melts for moderately SiO_2-rich melt compositions. These melts can crystallize abundant apatite during solidification and, thus, would be

effective agents for P-extraction during partial melting. Due to their very low apatite saturation concentration, the P-transport and storage capacity of granitic melts would be much more limited. An unexpected finding of this study are the substantial P and Mg contents in kyanite with 0.17-0.20 wt% P_2O_5 and 0.20-0.56 wt% MgO, respectively. The combined P-Mg incorporation into kyanite is consistent with the coupled substitution $^{[4]}Si^{4+} + {}^{[6]}Al^{3+} = {}^{[4]}P^{5+} + {}^{[6]}Mg^{2+}$ and with a strong preference of P for orthosilicate structures. The results of this study suggest that some to even all of the apatite now present in eclogites that underwent deep subduction formed by chemical adjustment of the eclogite garnet to decreasing $Na_3Al_2(PO_4)_3$-solubility during uplift and exhumation. This results in the appearance of apatite as a new phase in a hitherto apatite-free assemblage. Rapid transport to the surface and/or a lack of suitable reactants can suppress this re-equilibration and explain the occasionally high P- and Na-contents of eclogitic garnet-inclusions in diamond or garnets from diamondiferous eclogites sampled by kimberlites. Similarly, concurrent decreasing Ti-solubility in garnet may lead to rutile-saturation in eclogites that did not contain this phase under peak-*P* conditions as evidenced by the joint occurrence of (oriented) rutile and apatite inclusions in the eclogitic garnets. For the application of geothermobarometry, this delayed Ti (+P) saturation is important to be kept in mind.

key words: phosphorus, garnet, apatite, kyanite, eclogite, exhumation

INTRODUCTION

The transport and storage of P in the Earth's crust and upper mantle is characterized by an interplay between phosphate and silicate phases. The latter are represented by either solids or melts dependent upon the local *P-T* regime. Under crustal pressures and subsolidus temperatures, an essential portion of the bulk P budget for major rock types from the continental and oceanic crust, such as granites and granodiorites (0.02-0.18 wt% P_2O_5; e.g. Kemp and Hawkesworth 2004; Gao et al. 1998), MORBs (0.06-0.26 wt% P_2O_5; e.g. Klein 2004 and references), continental alkali-basalts (0.55-1.58 wt% P_2O_5; e.g. Farmer 2004) or andesites (0.18-0.23 wt% P_2O_5; e.g. Condie 1993), and their plutonic equivalents is stored in apatite. It is only in metapelites and granitic rocks with associated pegmatites that the REE-rich orthophosphates monazite and/or xenotime may be important as P carriers in addition to or instead of apatite (e.g. Bea 1996; Watt 1995; Spear and Pyle 2004). Pure hydroxyl- and fluorapatite is stable to 11-13 GPa at 1000-1500°C (Murayama et al. 1986) and, towards higher *P*, breaks down to form the anhydrous calcium phosphate tuite [γ-$Ca_3(PO_4)_2$] (Sugiyama and Tokonami 1987; Xie et al. 2003). In MORB-type bulk compositions the upper *P*-stability of hydroxyl-apatite is reduced to 7.0-7.5 GPa at 950°C as a result of tuite-forming reactions that involve apatite and phase components from the major eclogite phases garnet, coesite and clinopyroxene (Konzett and Frost 2009). During partial melting, the extent of the super-solidus stability of apatite largely depends upon the SiO_2 content of the melt. In SiO_2-rich (granitic) melts, apatite may remain stable up to moderate degrees of partial melting whereas in more silica-poor (e.g. basaltic) melts, even low degrees of partial melting are likely to completely remove apatite due to a much higher melt saturation concentration for P in basic compared to felsic melts (Watson 1979; Watson and Capobianco 1981). Under the subsolidus *P-T* conditions of the upper mantle and transition zone, silicates gradually become more important as hosts and transport media for P due to a *P*-(and *T*) induced increase in the P-solubility for silicate structures (Thompson 1975; Irving and Frey 1976; Brunet et al. 2006;

Hermann and Spandler 2007; Konzett and Frost 2009, Konzett et al. 2012). Amongst the common rock-forming silicates, garnet is by far the most important silicate-host for P with concentrations on the order of several hundred to several thousand µg/g as demonstrated in a number of experimental studies (see below). Based on this consistent experimental evidence one would expect to routinely find significant amounts of P and Na in garnet from UH*P* eclogites and UH*P* eclogite-facies felsic rocks and pelitic metasediments. With very few exceptions, however, this is not the case. The almost complete absence of Na-P-rich garnet from UH*P* assemblages, in particular from those containing apatite, indicates that P is efficiently transferred from garnet to other P-carriers during uplift and exhumation.

The present study was conducted to experimentally explore the mechanisms of P release from garnet during uplift and exhumation of UH*P* eclogites and its re-distribution within the eclogite assemblage by reacting a Na-P-rich garnet pre-synthesized under UH*P* conditions with a model eclogitic bulk composition under high pressure (H*P*) conditions and to assess the role that apatite and silicate phases (solids + melts) may play in this release/re-distribution process.

THE PHOSPHORUS STORAGE CAPACITY OF SILICATES IN HIGH-*P* ROCKS

As silicate phase substituent, P shows a strong preference for orthosilicate structures and is substituted for Si on tetrahedral sites. This preference for tetrahedral coordination makes P unique amongst highly charged (trace) elements. Whenever garnet is stable in a high-*P* silicate-dominated assemblage, this phase strongly fractionates P. High-*P*-*T* experiments performed with basaltic and metapelitic bulk compositions have shown that garnet coexisting with apatite contains 0.07-0.2 wt% P_2O_5 at *P* as low as 1.8 to 3.0 GPa. In the *P*-*T* range 4-13 GPa/1000-1350°C the P solubility in garnet strongly increases to ~0.4-0.6 wt% P_2O_5 (Thompson 1975; Hermann and Spandler 2007; Konzett and Frost 2009). P-contents in garnet not only increase with pressure but also with temperature although the *T*-effect is less

pronounced than that of *P* (Konzett and Frost 2009). In eclogites, high P contents in garnet are typically accompanied by elevated Na due to a coupled substitution $^{[8]}Na^{[4]}P^{[8]}M^{2+}{}_{-1}{}^{[4]}Si_{-1}$ (cf. Thompson 1975; Bishop et al. 1978; Haggerty et al. 1994) which may lead to a complete solid-solution between garnet and garnet-structured $Na_3Al_2(PO_4)_3$ (Thilo 1941; Brunet et al. 2006). At *P*>8 GPa additional Na may enter garnet through the coupled substitution $^{[8]}Na^{[6]}Si^{[8]}M^{2+}{}_{-1}{}^{[6]}Al_{-1}$ introducing a Na-majoritic component (Ringwood and Major 1971; Konzett and Frost 2009). Titanium which is a frequent additional minor constituent in eclogitic garnet, may be incorporated through the coupled substitutions $^{[8]}Na^{[6]}Ti^{[8]}M^{2+}{}_{-1}{}^{[6]}Al_{-1}$ or $^{[8]}Ca^{[6]}Ti^{[6]}Al_{-2}$ (Haggerty et al. 1994; Zhang et al. 2003a; Konzett and Frost 2009). It should be noted that high P contents in garnet do not *a priori* indicate high pressures of formation/equilibration because garnet from granitic rocks may contain P_2O_5 on a wt% level due to coupled substitutions $^{[8]}\square^{[4]}P_2{}^{[8]}M^{2+}{}_{-1}{}^{[4]}Si_{-2}$ and/or $^{[8]}Na^{[8]}\square^{[4]}P_3{}^{[8]}M^{2+}{}_{-2}{}^{[4]}Si_{-3}$ introducing vacancies on the M^{2+}-sites (Breiter et al. 2005).

Compared to garnet, the P storage capacity of clinopyroxene in eclogites is very limited. Experiments by Konzett and Frost (2009) yielded ≤ ~250 µg/g in the *P-T* range 3-15 GPa/900-1450°C. Data for P in omphacites from natural mantle eclogites (e.g. Bishop et al. 1978) are in agreement with these experimental results. Due to the very low P concentrations found in the eclogitic clinopyroxene, it has not been possible, so far, to unambiguously identify its incorporation mechanisms (cf. Mallmann et al. 2009 and references). For the extremely rare instances of P_2O_5 concentrations of >1 wt% P_2O_5 that are always associated with an extremely low f_{O2} for the host assemblage (Goodrich 1984; Zhitova et al. 2013), pyroxene compositional variations are consistent with a berlinite-type substitution $^{[4]}Al^{[4]}P^{[4]}Si^{4+}{}_{-2}$.

Very little is known about the P storage capacity of the SiO_2 polymorphs. For upper crustal *P-T* conditions, the scarce data available indicate very limited solubility in quartz on the order of <10-20 µg/g (Müller et al. 2003; Breiter et al. 2013). Under transition zone *P-T*

conditions, however, stishovite may contain significant P. Brunet et al. (2004) reported 0.5 wt% P_2O_5 in stishovite at 18 GPa and 1600°C and subsequent studies showed that P is present in stishovite in 6-fold coordination as the berlinite component (Brunet et al., 2007; Pellicer-Porres et al., 2007).

Although only rarely present in eclogites *sensu strictu*, titanite has to be included in the list of potential high-*P* carriers of P. Up to 0.3 wt% P_2O_5 have been reported for titanites containing oriented coesite and apatite-inclusions from ultra-high pressure (UH*P*) marbles of the Kokchetav Massif (Ogasawara et al., 2002) and up to 0.5 wt% P_2O_5 are present in titanites from coesite-bearing UH*P*-gneisses of the Dabieshan (Ye et al., 2002). The positive P-Al correlation displayed by these titanites would be consistent with a berlinite-type subsititution but cannot be confirmed based on the data presented due to the fact that Al is also involved in other substitutions such as $AlFTi_{-1}O_{-1}$.

EXPERIMENTAL STRATEGY

For the study of the decompression-induced P-redistribution in a eclogite assemblage containing P-Na-rich garnet, two starting materials were used: starting material-1 is a model eclogite in the system SiO_2-TiO_2-Al_2O_3-MgO-CaO-Na_2O which consists of a hypothetical mixture of 30% garnet ($prp_{90}grs_{10}$) + 60% clinopyroxene ($di_{80}jd_{10}en_{10}$) + 9% SiO_2 + 1% TiO_2 (cf. Konzett and Frost 2009) doped with 10% Na-P-rich garnet and 1% $Mg(OH)_2$ (bulk-I, Table 1). The garnet has an averaged formula $(Na_{0.04}Ca_{0.47}Mg_{2.53})Al_{1.98}[Si_{2.96}P_{0.04}]O_{12}$ and contains 0.3 wt% Na_2O and 0.7 wt% P_2O_5 (Table 1). Its composition was chosen to provide a significant $Na_3Al_2(PO_4)_3$ phase component that allows for accurate and precise Na and P analyses with the electron microprobe and promotes high reaction rates during the experiments.

The experimental approach adopted was to subject bulk-I to a pressure of 2 GPa at which the P-solubility/content of the $Na_3Al_2(PO_4)_3$ phase component in garnet is very low based on

179 the results of previous experimental studies. The temperatures of the experiments using bulk-I
180 range from 850°C, which is well below the solidus, to 1000°C, which is slightly above the
181 solidus. After the solidus had been located and the formation of apatite confirmed, an
182 additional run (JKI-149) was conducted to explore the effect on apatite-formation of the
183 temporal presence of a melt. In this run, the temperature was kept at 1000°C for 72 hours,
184 then cooled to 950°C at a cooling rate of 0.1°/min and then kept at 950°C for another ~400
185 hours. Starting material-II is a volatile-rich melt in the system SiO_2-TiO_2-Al_2O_3-MgO-CaO-
186 Na_2O-P_2O_5-H_2O (Table 1) that was generated by partial melting of bulk-I at 1000°C. It was
187 chosen as starting material in order to explore the capacity of melts formed by partial melting
188 of Na-P-rich garnet as transport media for P (and Na) and as possible sources of apatite during
189 crystallization.

190 It is important to emphasize that it was not the aim of the experiments to achieve a
191 complete equilibration at 2 GPa of the P-Na-rich garnet composition synthesized at 7 GPa and
192 to obtain an equilibrium P distribution in the model eclogite assemblages. In view of the
193 extremely sluggish cation diffusion in garnet such an attempt would be unrealistic under
194 typical eclogite facies *P-T* conditions. Instead, the experimental approach was designed to
195 trigger changes in phase compositions and phase assemblage that allow for the identification
196 of those reactions and phases that are most likely involved in the P-(Na)-loss from garnet and
197 subsequent P-redistribution during exhumation of an eclogite assemblage from UH*P*- to
198 shallow crustal *P-T* conditions.

199

200 ## EXPERIMENTAL AND ANALYTICAL METHODS

201 All starting materials were made from high-purity (≥99.99%) SiO_2, γ-Al_2O_3, TiO_2, MgO,
202 $CaCO_3$, and Na_2CO_3, $Ca_2P_2O_7$ (98%) and $Mg(OH)_2$ (≥95%). In a first step SiO_2, TiO_2, MgO,
203 $CaCO_3$, and Na_2CO_3 were mixed in appropriate proportions and these mixtures were stepwise
204 decarbonated by heating to 800°C with intermittent checks of the loss on ignition. In a second

step γ-Al_2O_3 and $Ca_2P_2O_7$, were added, the mixtures were homogenized in ethanol for another 20 minutes, dried and then stored at 120°C for further use.

The Na-P-rich garnet used for bulk-I was pre-synthesized at 7 GPa and 1200°C with a run duration of 134 hours using a 500t Walker-type multi anvil device at the University of Innsbruck. Details of the experimental procedure can be taken from Konzett and Frost (2009). After the experiment the sample capsule was removed from the assembly, embedded in epoxy resin, and ground down to expose the experimental charge for back-scattered electron (BSE) imaging and electron microprobe analysis (EMPA). After completion of the analytical work, the capsule content was removed, lightly crushed to break up the experimental charge into separate garnet grains and then mixed with the model eclogite oxide mix and with $Mg(OH)_2$ to prepare bulk-I. For bulk-II, the water was added using a micro-syringe immediately before welding of the sample capsule shut.

All experiments with bulk-I and -II were conducted at 2.0 GPa and 850-1000°C with Boyd-and-England-type piston cylinders using half-inch NaCl-pyrophyllite assemblages (Table 2). Both temperature and pressure were computer-controlled during the entire run duration to ±1°C and ±0.2 bar hydraulic oil pressure, the latter corresponding to ~100 bar sample pressure. After the experiments the sample capsules were removed from their assemblies, embedded longitudinally in epoxy and ground down to expose the centre of the experimental charge. The exposed surface was then polished for BSE-imaging, high-resolution compositional mapping and quantitative EMPA.

Phase compositions (Tables 3-5) were analyzed with a JEOL 8100 superprobe using 15 kV and variable beam current and measurement times on peaks and backgrounds of the X-ray lines as outlined below. The following standards were used: Si: natural quartz; Al, Mg and Ti: pure synthetic Al_2O_3, MgO and TiO_2; Ca, Na and P: natural diopside, jadeite and F-apatite; Na and P in garnet was analyzed with 20 nA beam current and 60 seconds/30 seconds on peaks and backgrounds of the X-ray lines. This yields detection limits of <100 µg/g and

231 relative 2σ errors for individual Na and P analyses on the order of ~7-23% for 1800-400 µg/g
232 Na and of ~7-16% for 2700-750 µg/g P, respectively. Clinopyroxene was analyzed in a two-
233 step procedure. Analyses were first performed with 20 nA beam current and 20 seconds/10
234 seconds on peaks/backgrounds of the X-ray lines. Wherever possible, an electron beam in
235 raster-mode was used to minimize Na diffusion. In cases where no raster could be used, the
236 beam current was reduced to 5 nA. In a second step, the clinopyroxene was re-analyzed using
237 a 150 nA beam current and 100 seconds/50 seconds on peaks/backgrounds of the P-Kα line.
238 This yields detection limits of <30 µg/g for P and relative 2σ errors for individual P analyses
239 on the order of ~20 to 6% for 100 to 500 µg/g P. Phosphorus in kyanite was analyzed using a
240 150 nA beam current and 100 seconds/50 seconds on peaks/backgrounds of the P-Kα line,
241 which results in detection limits of <20 µg/g and relative 2σ errors of ~3% for 800 µg/g P.
242 Melts turned out to be highly susceptible to beam damage and, consequently, were analyzed
243 with 5 nA beam current. This low beam current minimized, in part, but could not entirely
244 avoid beam damage in particular when the size of the melt pool, such as in run JKI-133,
245 precluded analyses with the electron beam in raster mode.

246 To quantify the modal amount of apatite, high-resolution and high-magnification BSE-
247 imaging of the experimental charges, combined with phase identification by EDX, was used.
248 Due to their bright appearance under BSE imaging and the strong Ca and P EDX-signal, it is
249 possible to unambiguously identify apatites as small as ~1 x 1 µm. In order to identify a
250 maximum of grains, the exposed areas of the experimental charges were subdivided into areas
251 of appropriate size and each area was searched for apatite. Clearly this method cannot ensure
252 that all apatites will be detected but it will yield a realistic approximation of the number of
253 apatites present within the area exposed. As a proxy for grain size, the longest and shortest
254 dimensions of individual apatite grains were measured and the two values were multiplied by
255 each other. As a measure of the frequency of apatite in the individual runs, the number of
256 apatite grains per 10000 μm^2 of exposed surface area (= 1 unit area or UA) of the

experimental charges was calculated along with the total area of all apatites per UA. This calculation only yields an approximation to the true modal amount of apatite in the experiments due to the extremely small grain size of many apatites and the simple method used to calculate the areas of the apatites.

RESULTS

Experimental textures and assemblages

Na-P-rich garnet. The garnet starting material recrystallized to form euhedral to rounded and compositionally homogeneous garnet grains ≤~30 μm in size. The only additional phase identified is kyanite that is present as isolated lath-shaped crystals with a modal amount of ~3% (Fig. 1a).

Bulk-I. At 2 GPa and 850°C (run JKI-116) bulk-I crystallizes garnet + clinopyroxene + quartz + minor orthopyroxene and magnesite + traces of rutile + apatite (Fig. 1b). Magnesite is inherited from the model eclogite starting material as a result of incomplete decarbonation and kyanite was most likely introduced through mixing of the Na-P-rich garnet with the model eclogite. With the exception of garnet all phases are, although mostly well crystallized, ≤10-20 μm in size and show a considerable variation in grain sizes. Garnet and the rare kyanite grains may reach 20-30 μm in size with occasional angular garnet fragments generated by crushing of the Na-P-garnet experimental charge prior to mixing with the model eclogite. Apatite is present as rounded to lath-shaped grains with grain sizes ranging from ≤1 x 1 to 24 x 6 μm mostly scattered in the pyroxene-garnet matrix as isolated grains or, more rarely, as inclusions in clinopyroxene. The average number of apatites identified is 2.7/UA with a total apatite area/UA of 22.7 μm^2 and the majority of the grains are ≤ ~3 μm in size (Fig. 2)

At 950°C and 975°C (runs JKI-118 and JKI-147; Figs. 1c, e) bulk-I crystallizes garnet + clinopyroxene + orthopyroxene + quartz + rutile + apatite. Orthopyroxene forms small

283 clusters of lath-shaped grains scattered in the garnet + clinopyroxene matrix and quartz is
284 present as irregular patches filling interstices beween clinopyroxene, orthopyroxene and
285 garnet. Compared to run JKI-116, the phases in JKI-118 and JKI-147, in particular
286 clinopyroxene, show less variation in their grain size and angular garnet fragments. Irregular
287 grain boundaries, such as those observed at 850°C, are rare. In both runs JKI-118 and JKI-
288 147, apatite textures and grain sizes (≤1 x 1 to 16 x 11 μm) are very similar to those
289 encountered at 850°C. But with 0.6/UA, the frequency of apatites is smaller than at 850°C.
290 Nevertheless, the total apatite area/UA in JKI-118 and JKI-147 is nearly identical with 18.6
291 and 18.1 7 μm^2, respectively. In JKI-147, large apatites may contain clinopyroxene inclusions
292 (Fig. 1e) and in JKI-118, apatite was also found as inclusions in garnet (Fig. 3).
293 In run JKI-133, conducted at 1000°C, small amounts of melt are present as tiny pools
294 rarely reaching ~10 μm in size interstitial between the matrix phases. Whereas rutile is still
295 stable, no apatite could be detected. (Fig. 1f).
296 Run JKI-149 was first kept at 1000°C, slightly above the solidus, and then cooled to
297 950°C for re-equilibration under subsolidus temperatures. This procedure results in the same
298 assemblage and textures for the major phases as observed in JKI-118, but has 1.8/UA and
299 more apatite with a higher proportion of grains ≤1 μm (Fig. 2) which results in a lower total
300 apatite area/UA of 13.5 μm^2. Unlike in JKI-118 apatites in JKI-149 may form small clusters
301 of several grains (Fig. 1d).
302 **Bulk-II.** In run JKI-141, conducted at 2 GPa and 800°C, abundant, quenched, vesicular
303 melt is present which coexists with quartz and clinopyroxene that both show grain sizes ≤ ~30
304 x 20 μm. Additional phases are needle-like kyanite and zoisite and accessory rutile. Apatite is
305 present as euhedral grains usually ≤5 μm in size either embedded in the quenched melt or as
306 inclusions in clinopyroxene (Fig. 1g). Two texturally distinct types of clinopyroxenes are
307 present (cf. Rossi 1988). Cpx-I forms the majority of the clinopyroxene and is present as lath-

to more irregularly shaped grains. Cpx-II is much rarer and forms lath- to needle-like grains intergrown with or enclosed within Cpx-I (Fig. 1h).

Phase composition

Garnet. In run JKI-116, conducted at 850°C, analyses of garnet with various grain sizes did not yield evidence for a significant change in composition, i.e. the garnet compositions analyzed are indistinguishable from the average composition of the garnet from run MA65 used as a constituent in bulk-I. At T ≥ 950°C garnet grains (≥10-15 μm in size) may show compositional zoning with Na-P-rich cores, representing the original garnet composition from MA65, and narrow rims with widths ≤~5 μm that are Na-P-depleted (0.05-0.14 wt% Na_2O; 0.16-0.31 wt% P_2O_5) and Ti-enriched (0.23-0.46 wt% TiO_2) (Figs. 3 and 4; Table 3). When normalized to 12 oxygens, P and Na apfu for individual garnet analyses are aligned close to a 1:1 trend line (Fig. 4c).

Pyroxenes. All analyzed clinopyroxene grains are diopside-jadeite solid solutions with minor Ca-Tschermak's pyroxene and enstatite contents that show little compositional variation within the *T*-range of the experiments with respect to their major element composition. All analyzed clinopyroxene grains contain significant P with averaged concentrations between 341 and 159 μg/g (Fig. 5). In run JKI-141, the coexisting clinopyroxenes have averaged compositions $jd_{30}di_{49}Cats_{08}en_{01}CaEs_{06}$ (cpx-I) and $jd_{14}di_{79}Cats_{02}en_{02}CaEs_{03}$ (cpx-II), respectively (Table 4). Due to their very small grain size, only a few orthopyroxene grains could be analyzed without risking beam overlap with adjacent phases. Their P contents are lower than those of the coexisting clinopyroxenes (Fig. 5). Ca-in-orthopyroxene thermometry (Brey and Köhler 1990), applied to runs JKI-118 and JKI-147, yields 945°C for both, which is in good agreement with actual run temperatures.

Apatite. The few apatite grains large enough for EMPA contain MgO in the range 0.7-1.1 wt%, which is consistent with results from previous studies on apatite chemistry at high *P*

and *T* (e.g. Konzett and Frost, 2009). All analyzed apatites also show variable Cl contents of up to ~3.6 wt% (Table 5), which result from Cl introduced either through the starting materials or from the laboratory atmosphere.

Kyanite and melt. In runs JKI-116 (bulk-I) and JKI-141 (bulk-II), kyanite contains significant amounts of P_2O_5 and MgO in the range 0.16-0.24 wt% and 0.22-0.62 wt%, respectively (Table 3). Kyanite from JKI-133 also contains 0.27-0.54 wt% TiO_2. High-resolution compositional mapping shows a homogeneous P-distribution in kyanite from JKI-116 and a patchy P-, Mg-, and Ti-distribution in kyanite from JKI-133 (Fig. 6).

The melt in run JKI-133 (bulk-I) contains 61.0 wt% SiO_2 and 14.5 wt% Al_2O_3 with an average Al saturation index (ASI) of 1.5 and 0.7 wt% P_2O_5. Analytical totals of ~84 wt% indicate a significant volatile content consisting in large part of H_2O. Because bulk-I contains some CO_2 as a result of incomplete decarbonation of the starting material as evidenced by the presence of magnesite in run JKI-116, it must be assumed that the melt contains CO_2 in addition to H_2O. In the preparation of bulk-II, since it could not be determined quantitatively, this CO_2 content was neglected. The melt in run JKI-141 (bulk-II) at 800°C contains 65.6 wt% SiO_2 and 13.6 wt% Al_2O_3 with ASI = 1.1 and has a very low P_2O_5 content of 0.07 wt%. Its analytical total of ~87 wt% and vesicular texture indicate H_2O-saturation. Melts from both JKI-133 and JKI-141 contain small amounts of Cl in the range ~0.2-0.3 wt% as a result of a trace Cl contamination of the bulk mix (Table 3).

DISCUSSION

Phosphorus in garnet from UH*P*-eclogite assemblages

As outlined above, high *P-T* experiments consistently show that garnet in basaltic and pelitic systems with sufficiently high bulk P contain on the order of one to several tenth wt% P_2O_5 and Na_2O at *P-T* conditions typical for the (U)H*P* eclogite facies. Hence, if it is assumed that the composition of garnet from natural eclogites is not significantly different from that

equilibrated under peak metamorphic *P-T* conditions, than similarly high P_2O_5 and Na_2O contents should be expected in virtually every eclogite garnet. Although a large number of studies are available on the composition of UH*P* eclogite phases, and in particular on that of garnet, EMPA of garnet does not routinely include P so that the number of analyses that report P in addition to Na and Ti is extremely limited. When at least Na_2O and TiO_2 contents of garnet are reported, their concentration is usually <0.10 to 0.05 wt%, which would require a detailed description of the EMPA analytical conditions in order to properly judge the statistical significance of these numbers. This information, however, is not always provided. Nevertheless, a sufficiently clear pattern of the P concentration in garnet from UH*P* eclogites emerges from the data reviewed.

Eclogite garnet from UH*P* mantle settings occurs as inclusions in diamonds or as constituent of xenoliths sampled by kimberlites. P and Na contents reported for this type of garnet ranges from <0.02-0.14 wt% P_2O_5 and <0.02-0.40 wt% Na_2O (Reid et al. 1976; Smyth and Hatton 1977; Bishop et al. 1978; McDade and Harris 1998; Taylor et al. 2003; Stachel et al. 1998, 2004; Anand et al. 2004; Tappert et al. 2005). A sizable number of the garnet analyses show ≥0.08 wt% P_2O_5 and ≥0.10 wt% Na_2O with the highest values reported for diamond inclusions from Namibian alluvial diamonds (Stachel et al. 2004).

For crustal UH*P* eclogites, and associated metasediments/metaplutonic rocks, the number of garnet analyses reporting P in addition to Na is even more limited with P_2O_5 and Na_2O contents in the range ≤0.03-0.09 wt% and <0.05-0.22 wt%, respectively (Bryhni et al. 1968; Carswell et al. 2000; Vrana and Fryda 2003). As an exception, Carswell et al. (2000) report 0.25 wt% P_2O_5 and 0.27 wt% Na_2O for garnet from a Dabie Shan UH*P* orthogneiss. If P is not analyzed, then Na can be used at least as a proxy for P provided that the Ti content of the garnet is known and the presence of apatite ensures saturation of the bulk with P. Elevated P contents in garnet, as a result of the coupled substitution $^{[8]}Na^{[4]}P^{[8]}M^{2+}{}_{-1}{}^{[4]}Si_{-1}$, is indicated by high Na contents with Na>>Ti apfu and no indication for high Y, REE that would enable

386 $^{[8]}Na^{[8]}(Y, REE)^{[8]}M^{2+}_{-2}$ (Enami et al.1995). Almost all garnet analyses reviewed for this study
387 show ≤0.05-0.08 wt% Na_2O (e.g. Tong et al. 2007; Okay 1993; Song et al. 2003; Zhang et al.
388 2003b; Xia et al. 2005; Nowlan et al. 2000; Zeming et al. 2000; Katayama et al. 2006;
389 Carswell et al. 2000; Parkinson 2000) and even those with higher Na (e.g. Zhang et al. 1997)
390 have sufficient Ti to explain Na-incorporation entirely by $^{[8]}Na^{[6]}Ti^{[8]}M^{2+}_{-1}{}^{[6]}Al_{-1}$. Of the
391 studies reviewed, only two (Zhang et al. 2009; Perchuk 2008) report Na-rich garnet with 0.13-
392 0.24 wt% Na_2O that would satisfy the criteria for potentially high P. Hence it seems that the
393 majority of garnets from crustal UH*P* eclogites has negligible P. In summary this literature
394 review indicates that garnet with P contents well above the detection limit of routine EMPA
395 analyses is very rare in both crustal and mantle UH*P* eclogites and associated metasediments
396 and metaplutonic (granitic) rocks. When present, P is almost always accompanied by elevated
397 Na contents which is consistent with a coupled P-Na substitution favored by high pressures as
398 observed in high-*P*-*T* experiments.
399
400 **The role of apatite and melt as P-carriers during exhumation of UH*P* rocks**
401 The experiments conducted in a model eclogite bulk system show that under subsolidus
402 *P*-*T* conditions both P and Na are very quickly and efficiently released from garnet if the
403 eclogite is exposed to decreasing pressures and temperatures during uplift and exhumation in
404 the wake of subduction. Unambiguous evidence for this P release is provided by newly
405 formed apatite and by the P contents in both pyroxenes and kyanite.
406 The Na-P depleted rims around Na-P-rich garnet grains (Figs. 3 and 4) can be explained
407 as the combined result of compositional adjustment and growth of garnet. It should be noted
408 that the model eclogite, represented by bulk-I, crystallizes garnet over a large *P*-*T* range (cf.
409 Konzett and Frost 2009). Hence, not only partial breakdown of P-Na-rich garnet to supply P
410 for apatite, pyroxenes, and kyanite but also neo-formation of garnet must take place during
411 the experiments. Low magnification compositional mapping, however, did not show any P-

412 Na-free garnet grains ≥ ~3 to 5 μm in size. This indicates that the nucleation of garnet is
413 energetically less favorable than garnet growth using pre-existing garnet as a nucleation site.
414 The P-Na-depleted and Ti-enriched garnet-rims that appear with increasing frequency at *T*
415 ≥950°C thus represent an approach to a Na-P-free and Ti-bearing garnet composition typical
416 for crustal eclogite-facies *P-T* conditions in a Ti-saturated bulk system. Molar Na:P ratios
417 close to 1:1 in both P-rich cores and P-poor rims (Fig. 4) further indicate that the transition
418 from UH*P*- to H*P* garnet compositions under subsolidus conditions is accompanied by a loss
419 of a $Na_3Al_2(PO_4)_3$-component that is involved in reactions responsible for concurrent apatite-
420 formation. In the experiments the water required for apatite formation was added through
421 brucite. In natural eclogites, water can be supplied during uplift and exhumation either from
422 external sources or by exsolution of structurally bound hydrogen from nominally anhydrous
423 eclogite phases such as clinopyroxene, garnet, or rutile that typically contain several hundred
424 μg/g H_2O (e.g. Katayama et al. 2006; Xia et al. 2005). Aside from water, eclogitic apatite
425 typically contains significant F and Cl (e.g. Haggerty et al. 1994, Svensen et al. 2001, Miller
426 et al. 2007, Konzett et al. 2011) whose concentrations are complex functions of *P, T,* the bulk
427 P content, and H_2O/halogen-ratios. The thermodynamic model devised by Patiño Douce et al.
428 (2011) predicts that high F contents are favored by high temperatures and low bulk P contents
429 whereas high Cl contents are favored by high Cl contents of the coexisting fluid but are not
430 significantly influenced by *T*. Hence it can be assumed that within the *P-T* range typical for
431 eclogites Cl has little influence on the thermal stability of apatite.

432 In the simplified chemical system P_2O_5-SiO_2-Al_2O_3-MgO-CaO-Na_2O-H_2O used for the
433 experiments, in which clinopyroxene, garnet, SiO_2, apatite, and fluid are represented by the
434 phase components jadeite (jd), diopside (di), enstatite (en), pyrope (prp), grossular (grs), Na-
435 P-garnet [$Na_3Al_2(PO_4)_3$], SiO_2, apatite (ap) and H_2O, the following apatite-forming reactions
436 are possible:
437

438 1) 2 NaP-grt + 2 SiO_2 + grs + 7 di + H_2O = 2 ap + 6 jd + 7 en

439 (2) 2 NaP-grt + 2 SiO_2 + prp + 10 di + H_2O = 2 ap + 6 jd + 13 en

440 (3) 12 NaP-grt + 12 SiO_2 + 13 grs + 21 di + 6 H_2O = 12 ap + 7 prp + 36 jd

441 (4) 6 NaP-grt + 6 SiO_2 + 10 grs + 21 en + 3 H_2O = 6 ap + 7 prp + 18 jd

442

443 Based on a positive slope for the reaction grs + 3 en = prp + 3 di, a possible arrangement of
444 these reactions with respect to *P* and *T* are shown in Fig. 7. The reaction stoichiometries
445 indicate that in an eclogite, the P transfer from garnet to apatite is associated with the
446 consumption of SiO_2 and an increase in Na in the coexisting omphacite.

447 In the subsolidus experiments, apatite nucleation preferentially takes place in the
448 interstitial matrix between pyroxene and garnet or as inclusions in clinopyroxene with a ±
449 homogeneous distribution of apatite throughout the experimental charges. In rare instances
450 apatite may also appear as inclusions in garnet as shown in Fig. 3. The grain size distribution
451 of apatite is variable with a higher proportion of very small grains in runs JKI-116 and JKI-
452 149 (Fig. 2). A comparison of runs JKI-118 and JKI-149 suggests that the temporary presence
453 of small amounts of melt in an eclogite containing Na-P-rich garnet promotes nucleation of
454 apatite.

455 Low-degree partial melting of bulk-I at 2 GPa/1000°C produces a P-rich hydrous melt
456 with 0.7 wt% P_2O_5 and ~61 wt% SiO_2, respectively, which is apatite undersaturated.
457 Equilibration of this melt composition at 800°C generates abundant apatite coexisting with
458 clinopyoxene + quartz + kyanite + zoisite + rutile (Fig. 1g). This shows that initially apatite-
459 undersaturated melts can be effective agents for P-extraction from eclogites containing P-rich
460 garnet under subsolidus *P-T* conditions. Phosphorus contents on a wt% level resulting from
461 high apatite saturation P_2O_5 concentrations are, however, only possible in melts with low to
462 moderate (e.g. dioritic) SiO_2 contents (Watson 1979; Watson and Capobianco 1981; Green
463 and Watson 1982). High *P-T* partial melting experiments using various natural eclogite

compositions as starting materials produce melts with ~52-77 wt% SiO_2 (Rapp et al. 1991; Sen and Dunn 1994; Pertermann and Hirschmann 2003; Spandler et al. 2008; Laurie and Stevens 2012). Thus, at least some of the partial melt compositions fall into the range of SiO_2 contents for which a high P storage capacity would be plausible. In H_2O-bearing eclogites and at sufficiently high but still poorly constrained pressures (≥~3.5 GPa; Zheng et al. 2011), progressive heating, with attendant dehydration, does no longer produce melts but supercritical silicate-rich fluids with a highly complex composition for which P_2O_5 concentrations of several wt% were reconstructed (cf. Ferrando et al. 2005). These fluids would clearly be as suitable for P-transport and re-distribution as melts.

Phosphorus in kyanite?

Kyanite has traditionally been considered a phase that, aside from occasionally significant Cr and Fe^{3+} contents (e.g. Pivin et al. 2011 and references), has little to offer in terms of compositional variability. Hence, little to no attention has been paid to kyanite as a potential source of petrogenetic information based on its minor/trace element content. It is only very recently that attempts were made to use subtle variations in the transition metal content of kyanite to extract such information (Horkley et al. 2013). In view of this reputed compositional simplicity, significant averaged P and Mg contents for kyanite from runs JKI-116 and JKI-141 of 0.17-0.20 wt% P_2O_5 and 0.22-0.56 wt% MgO (Table 3, Fig. 6) came as a surprise. The possibility that P and Mg in kyanite are analytical artefacts as a result of secondary fluorescence or beam-overlap with adjacent P-rich phases can be ruled out based on the grain size of the kyanite grains analyzed (cf. Brunet and Chazot 2001; Konzett et al. 2012). A coupled substitution scheme that can explain the elevated P and Mg would be $^{[4]}Si^{4+} + {}^{[6]}Al^{3+} = {}^{[4]}P^{5+} + {}^{[6]}Mg^{2+}$. Incorporation of P into kyanite would also be consistent with the strong preference of P for orthosilicate structures. The higher Mg contents in kyanite from JKI-141, compared to JKI-116, are accompanied by significant Ti which is consistent with an

additional coupled substitution $2^{[6]}Al^{3+} = {}^{[6]}Ti^{4+} + {}^{[6]}Mg^{2+}$. It should be noted that when normalized to 5 oxygens the kyanite formulae always show an excess of Mg compared to P or P+Ti (Table 3). This indicates that the excess Mg takes part in additional substitutions possibly involving H (cf. Wieczorek et al. 2003, 2004).

In case of JKI-116, kyanite was most likely introduced into bulk-I together with the Na-P-rich garnet (cf. Fig. 1a) and originally formed at 7 GPa and 1200°C. If it is assumed that P-diffusion in kyanite is as sluggish as in olivine (Watson and Cherniak 2014) then the high P and Mg contents in kyanite from JKI-116 may reflect its ability to incorporate P and Mg under UH*P* conditions similar to the behaviour of garnet in which Na is coupled to P but are not necessarily equilibrium contents at 2 GPa and 850°C. Although no data for P in kyanite are available from the literature it is worth noting that kyanite with 0.26-0.55 wt% MgO has been reported as inclusions in diamonds (Smith et al. 2009; Bulanova et al. 2010). The more irregularly distributed P and Mg contents in non-inherited kyanite from run JKI-141 (Fig. 6) might well be disequilibrium values which result from rapid and variable growth rates combined with sluggish P diffusion (cf. Milman-Barris et al. 2008). Again a virtually non-existant database on minor and trace elements in both H*P*- and UH*P*-kyanite at present does not allow for a comparison of natural and experimental kyanite compositions. Clearly, more experiments are required to investigate the *P*-*T*-bulk compositional systematics of P solubility in kyanite. Nevertheless, the admittedly preliminary results of this study suggest that P should be considered as a potential minor to trace element constituent of kyanite. They also lend support to the notion that minor/trace element analyses of kyanite would be more rewarding than hitherto assumed.

IMPLICATIONS

Apatite is a very common accessory minertal of both UH*P* and HP eclogites (e.g. Tong et al. 2007; Okay 1993; Song et al. 2003; Zhang et al. 2003b; Xia et al. 2005; Nowlan et al.

2000; Zeming et al. 2000; Katayama et al. 2006; Schmädicke et al. 1992). It typically occurs as rounded grains scattered between the major eclogite phases. One peculiar textural variety of apatite reported from eclogites equilibrated under UH*P* conditions are (oriented) apatite rods in garnet and/or clinopyroxene that are often associated with rutile-needles and, more rarely with SiO_2-polymorphs, kyanite, and ilmenite (e.g. Fung and Haggerty 1995; Ye et al. 2000; Zhang et al. 2003a; Yang and Liu 2004; Alifirova et al. 2013, 2015; Ruiz-Cruz and Sanz 2013; Glassley et al. 2014; Axler and Ague 2015). The apatite textures produced in the present study provide direct experimental evidence for a possible subsolidus origin of all textural types of apatite encountered in UH*P*-eclogites, namely matrix apatite as well as inclusions in garnet and clinopyroxene, from decompression and cooling-induced release of a $Na_3Al_2(PO_4)_3$-component from garnet in the presence of a hydrous fluid. This confirms the idea of Fung and Haggerty (1995) that garnet is a likely P-source for apatite formation in eclogites. It should be kept in mind that even at *P* as low as 2.5 to 3 GPa, garnets may contain significant P and Na (Hermann and Spandler 2008, Konzett and Frost 2009). Thus, in order to explain the extremely low P and Na contents that are typical for garnet in eclogites emplaced at crustal levels, a combination of decompression *and* cooling is required. Hence, dependent upon the bulk P-content of the rock, the depth of burial and the extent of cooling, some to all of the apatite in eclogites that underwent deep subduction were not part of the equilibrium eclogite assemblage under peak metamorphic *P-T* conditions but likely formed during exhumation and subsequent chemical adjustment of the eclogitic garnet to decreasing $Na_3Al_2(PO_4)_3$-solubility. For example at pressures of 4-6 GPa, P_2O_5 solubilities in eclogitic garnet and clinopyroxene are ~0.25 wt% and ~0.039 wt% (=170 µg/g P), respectively (cf. Konzett and Frost 2009). If it is assumed that an eclogite contains 30% garnet and 60% clinopyroxene, then any such eclogite with <~0.10 wt% bulk P_2O_5 content would not contain apatite at depths of 120-180 km because all the P could be stored in garnet and clinopyroxene. For bulk P_2O_5 contents of 0.20-0.25 wt%, ~30-40% of the apatite present after exhumation

and emplacement in the crust could have formed from P released from garnet. In spite of its very low P-content, compared to garnet, even clinopyroxene, when present as major constituent of an eclogite assemblage, can contribute to apatite formation during exhumation to a non-negligible extent (cf. Table 6). Rapid transport to the surface, and/or a lack of suitable reactants, can suppress garnet re-equilibration and explain the occasionally high P- and Na-contents of eclogitic garnet inclusions in diamond or of garnet from diamondiferous eclogites sampled by kimberlites (e.g. Stachel et al., 2004; Reid et al., 1976). In the case of the high P-Na garnet reported by Carswell et al. (2000) from UH*P* orthogneisses, their tectonic history involving extensive mid crustal equilibration at ~400-450°C/6 kbar would be consistent with P incorporation by $^{[8]}Na^{[8]}\square^{[4]}P_3{}^{[8]}M^{2+}{}_{-2}{}^{[4]}Si_{-3}$ under low pressures as observed by Breiter et al. (2005).

Similar considerations apply to Ti in garnet for which decreasing solubility of $M_3(CaTi)Si_3O_{12}$ and/or $NaCa_2(AlTi)Si_3O_{12}$ phase components (Zhang et al. 2003a) during exhumation may lead to the formation of rutile in a hitherto TiO_2-undersaturated assemblage. In fact, both apatite and rutile may coexist as oriented inclusions in garnet (e.g. Fung and Haggerty 1995; Zhang et al. 2003a). The possibility that TiO_2-saturation may be reached only after the *P*-(*T*) peak of metamorphism has important implications for the application of geothermometers that rely on a TiO_2-saturated assemblage such as Ti-in-zircon or Zr-in-rutile.

ACKNOWLEDGEMENTS

Thoughtful comments and suggestions by two anonymous reviewers and by Dan Harlov helped to improve the quality of the manuscript. Their contributions are gratefully acknowledged.

REFERENCES CITED

Alifirova, T.A., and Pokhilenko, L.N. (2013) Apatite exsolution as an indicator of Udachnaya grospydite UHP history. Goldschmidt2013 Conference Abstracts, 576.

Alifirova, T.A., Pokhilenko, L.N., and Korsakov, A.V. (2015) Apatite, SiO2, rutile and orthopyroxene precipitates in minerals of eclogite xenoliths from Yakutian kimberlites, Russia. Lithos, 226, 31-49.

Anand, M., Taylor, L.A., Misra, K.C., Carlson, W.D., and Sobolev, N.V. (2004) Nature of diamonds in Yakutian eclogites: views from eclogite tomography and mineral inclusions in diamonds. Lithos, 77, 333-348.

Axler, J.A., and Ague, J.J. (2015) Exsolution of rutile or apatite precipitates surrounding ruptured inclusions in garnet from UHT and UHP rocks. Journal of metamorphic Geology, doi:10.1111/jmg.12145.

Bea, F. (1996) Residence of REE, Y, Th and U in granites and crustal protoliths; implications for the chemistry of crustal melts. Journal of Petrology, 37, 521-552.

Bishop, F.C., Smith, J.V., and Dawson, J.B. (1978) Na, K, P and Ti in garnet, pyroxene and olvine from peridotite and eclogite xenoliths from African kimberlites. Lithos, 11, 155-173.

Breiter, K., Novák, M., Koller, F., and Cempírek, J. (2005) Phosphorus – an omnipresent minor element in garnet of diverse textural types from leucocratic grenitic rocks. Mineralogy and Petrology, 85, 205-221.

Breiter, K., Ackerman, L., Svojtka, M., and Müller, A. (2013) Behavior of trace elements in quartz from plutons of different geochemical signature: A case study from the Bohemian Massif, Czech Republic. Lithos, 175-176, 54-67.

591 Brey, G.P., and Köhler, T. (1990) Geothermobarometry in four-phase lherzolites II. New
592 thermobarometers, and practical assessment of existing thermometers. Journal of
593 Petrology, 31, 1353-1378.
594 Brunet, F., and Chazot, G. (2001) Partitioning of phosphorus between olivine, clinopyroxene
595 and silicate glass in a spinel lherzolite xenolith from Yemen. Chemical Geology, 176, 51-
596 72.
597 Brunet, F., Irifune, T., Sanehira, T., Ymazaki, D., and Shinmei, T. (2004) HP and HT
598 polymorphism of $AlPO_4$ and its solubility in SiO_2-stishovite: implications for phosphorus
599 geochemistry. American Geophysical Union, Fall Meeting 2004, abstract#V41C-1414.
600 Brunet, F., Bonneau, V., and Irifune, T. (2006) Complete solid-solution between
601 $Na_3Al_2(PO_4)_3$ and $Mg_3Al_2(SiO_4)_3$ garnets at high pressure. American Mineralogist, 91,
602 211-215.
603 Brunet, F., Flank, A.-M., Itié, J.-P., Irifune, T., and Lagarde, P. (2007) Experimental evidence
604 of sixfold oxygen coordination for phosphorus. Amercan Mineralogist, 92, 989-993.
605 Bryhni, I., Bollingberg, H.J., and Graff, P.-R. (1968) Eclogites in quartzo-feldspathic gneisses
606 of Nordfjord, West Norway. Norsk Geologisk Tidsskrift, 49, 193-225.
607 Bulanova, G.P., Walter, M.J., Smith, C.B., Kohn, S.C., Armstrong, L.S., Blundy, J. and
608 Gobbo, L. (2010) Mineral inclusions in sublithospheric diamonds from Collier 4
609 kimberlite pipe, Juina, Brazil: subducted protoliths, carbonated melts and primary
610 kimberlite magmatism. Contributions to Mineralogy and Petrology, 160, 489-510.
611 Carswell, D.A., Wilson, R.N., and Zhai, M. (2000) Metamorphic evolution, mineral chemistry
612 and thermobarometry of schists and orthogneisses hosting ultra-high pressure eclogites in
613 Dabieshan of central China. Lithos, 52, 121-155.
614 Condie, K. C. (1993) Chemical composition and evolution of the upper continental crust:
615 contrasting results from surface samples and shales. Chemical Geology, 104, 1-37.

616 Enami, M., Cong, B., Yoshida, T., and Kawabe, I. (1995) A mechanism for Na incorporation
617 in garnet: An example from garnet in orthogneiss from the Su-Lu terrane, eastern China.
618 American Mineralogist, 80, 475-482.
619 Farmer, G.L. (2004) Continental basaltic rocks. In H. D. Holland and K. K. Turekian, Eds.,
620 Treatise on Geochemistry, vol. 3, Elsevier, Amsterdam, 85-121.
621 Ferrando, S., Frezzotti, M.L., Dallai, L., and Compagnoni, R. (2005) Multiphase solid
622 inclusions in UHP rocks (Su-Lu, China): Remnants of supercritical silicate-rich aqueous
623 fluids released during continental subduction. Chemical Geology 12/2005; DOI:
624 10.1016/j.chemgeo.2005.01.029
625 Finger, L.W., and Burt, D.M. (1972) REACTION, a FORTRAN IV computer program to
626 balance chemical reactions. Carnegie Institution Yearbook, 71, 616-620.
627 Fung, A.T., and Haggerty, S.E. (1995) Petrography and mineral compositions of eclogites
628 from the Koidu Kimberlite Complex, Sierra Leone. Journal of Geophysical Research,
629 100, 20451-20473.
630 Gao, S., Luo, T.-C., Zhang, B.-R., Zhang, H.-F., Han, Y.-W., Zhao, Z.-D., and Hu, Y.-K.
631 (1998) Chemical composition of the continental crust as revealed by studies in East
632 China. Geochimica et Cosmochimica Acta, 62, 1959-1975.
633 Glassley, W.E., Korstgård, J.A., Sørensen, K., and Platou, S.W. (2014) A new UHP
634 metamorphic complex in the 1.8 Ga Nagssugtoqidian Orogen of West Greenland.
635 American Mineralogist, 99, 1315-1334.
636 Goodrich, C.A. (1984) Phosphoran pyroxene and olivine in silicate inclusions in natural iron-
637 carbon alloy, Disko Island, Greenland. Geochimica et Cosmochimica Acta, 48, 1115-
638 1126.
639 Green, T.H., and Watson, E.B. (1982) Crystallization of apatite in natural magmas under high
640 pressure, hydrous conditions, with particular reference to “orogenic” rock series.
641 Contributions to Mineralogy and Petrology, 79, 96-105.

642 Haggerty, S.E., Fung, A.T., and Burt, D.M. (1994) Apatite, phosphorus and titanium in
643 eclogitic garnet from the upper mnatle. Geophysical Research Letters, 21, 1699-1702.
644 Hermann, J., and Spandler, J.C. (2007) Sediment melts at sub-arc depth: an experimental
645 study. Journal of Petrology, 49, 717-740.
646 Horkley, L.K., Spear, F.S., Ruscitto, D.M., and Tailby, N.D. (2013) The secret life of kyanite.
647 The Geological Society of America, 48th Annual Meeting, paper no. 43-1; available under
648 http://gsa.confex.com/gsa/2013NE/webprogram/Paper215738.html
649 Irving, A.J., and Frey, F.A. (1976) Effect of composition on the partitioning of rare earth
650 elements, Hf, Sc and Co between garnet and liquid. Eos, 57, 339.
651 Katayama, I., Nakashima, S., and Yurimoto, H. (2006) Water content in natural eclogite and
652 implication for water transport into the deep upper mantle. Lithos, 86, 245-259.
653 Kemp, A.I.S. and Hawkesworth, C.J. (2004) Granitic perspectives on the generation and
654 secular evolution of the continental crust. In H. D. Holland and K. K. Turekian, Eds.,
655 Treatise on Geochemistry, vol. 3, Elsevier, Amsterdam, 349-410.
656 Klein, E. M. (2004) Geochemistry of the igneous oceanic crust. In H. D. Holland and K. K.
657 Turekian, Eds., Treatise on Geochemistry, vol. 3, Elsevier, Amsterdam, 433-463.
658 Konzett, J., and Frost, D.J. (2009) The high P-T stability of hydroxyl-apatite in natural and
659 simplified MORB – an experimental study to 15 GPa with implications for transport and
660 storage of phosphorus and halogens in subduction zones. Journal of Petrology, 50, 2043-
661 2062.
662 Konzett, J., Krenn, K., Hauzenberger, Ch., Whitehouse, M. and Hoinkes, G. (2011) High
663 pressure tourmaline formation and fluid activity in Fe-Ti-rich eclogites from the
664 Kreuzeck Mountains, Eastern Alps, Austria. Journal of Petrology, 53, 99-125.
665 Konzett, J., Rhede, D., and Frost, D.J. (2012) The high PT stability of apatite and Cl
666 partitioning between hydrous potassic phases in peridotite: an experimental study to 19

667 GPa with implications for the transport of P, Cl and K in the upper mantle. Contributions
668 to Mineralogy and Petrology, 163, 277-296.
669 Laurie, A. and Stevens, G. (2012) Water-present eclogite melting to produce Earth's early
670 felsic crust. Chemical Geology, 314-317, 83-95.
671 Mallmann, G., O'Neill, H. St. C., and Klemme, S. (2009) Heterogeneous distribution of
672 phosphorus in olivine from otherwise well-equilibrated spinel peridotite xenoliths and its
673 implications form the mantle geochemistry of lithium. Contributions to Mineralogy and
674 Petrology, DOI 10.1007/s00410-009-0393-6
675 McDade, P., and Harris, J.W. (1998) Syngenetic inclusion bearing diamonds from Letseng-la-
676 Terai, Lesotho. In J.J. Gurney, J.L. Gurney, M.D. Pascoe, and S.H. Richardson, Eds.,
677 Proceedings of the VIIth International Kimberlite Conference; Red Roof Design cc, Cape
678 Town, South Africa, pp. 557-566.
679 Miller, C., Zanetti, A., Thöni, M. and Konzett, J. (2007) Eclogitisation of gabbroic rocks:
680 Redistribution of trace elements and Zr in rutile thermometry in an Eo-Alpine subuction
681 zone (Eastern Alps) Chemical Geology, 239, 96-123.
682 Milman-Barris, M.S., Beckett, J.R., Baker, M.B., Hofman, A.E., Morgan, Z., Crowley, M.R.,
683 Vielzeuf, D., and Stolper, E. (2008) Zoning of phosphorus in igneous olivine.
684 Contributions to Mineralogy and Petrology, 155, 739-765.
685 Müller, A., Wiedenbeck, M., Van den Kerkhof, A.M., Kronz, A., and Simon, K. (2003) Trace
686 elements in quartz – a combined electron microprobe, secondary ion mass spectrometry,
687 laser-ablation ICP-MS, and cathodoluminescence study. European Journal of
688 Mineralogy, 15, 747-763.
689 Murayama, J.K., Nakai, S., Kato, M., and Kumazawa, M. (1986) A dense polymorph of
690 $Ca_3(PO_4)_2$: a high pressure phase of apatite decomposition and its geochemical
691 significance. Physics of the Earth and Planetary Interiors, 44, 293-303.

692 Nowlan, E.U., Schertl, H.-P., and Schreyer, W. (2000) Garnet-omphacite-phengite
693 thermobarometry of eclogites from the coesite-bearing unit of the southern Dora-Maira
694 Massif, Western Alps. Lithos, 52, 197-214.
695 Ogasawara, Y., Fukusawa, K., and Maruyama, S. (2002) Coesite exsolution from supersilicic
696 titanite in UHP marble from the Kokchetav Massif, northern Kazakhstan. American
697 Mineralogist, 87, 454-461.
698 Okay, A.I. (1993) Petrology of a diamond and coesite-bearing metamorphic terrain: Dabie
699 Shan, China. European Journal of Mineralogy, 5, 659-675.
700 Parkinson, C.D. (2000) Coesite inclusions and prograde compositional zonation of garnet in
701 whiteschist of the HP-UHPM Kokchetav massif, Kazakhstan: a record of progressive
702 UHP metamorphism. Lithos, 52, 215-233.
703 Patiño Douce, A.E., Roden, M.F., Chaumba, J., Fleisher, C. and Yogodzinki, G. (2011)
704 Compositional variability of terrestrial mantle apatites, thermodynamic modeling of
705 apatite volatile contents, and the halogen and water budgets of planetary mantles.
706 Chemical Geology, 288, 14-31.
707 Pellicer-Porres, J., Saitta, A.M., Polian, A., Itié, J.-P., and Hanfland, M. (2007) Six-fold-
708 coordinated phosphorus by oxygen in $AlPO_4$ quartz homeotype under high pressure.
709 Nature Materials, 6, 698-702.
710 Perchuk, A.L. (2008) Unusual inclusions in garnet from the diamond-bearing gneiss of the
711 Erzgebirge, Germany. Geochemistry International, 46, 296-303.
712 Pertermann, M. and Hirschmann, M.M. (2003) Anhydrous partial melting experiments on
713 MORB-like eclogite: phase relations, phase compositions and mineral-melt partitioning
714 of major elements at 2-3 GPa. Journal of Petrology, 44, 2173-2201
715 Pivin, M., Berger, J., and Demaiffe, D. (2011) Nature and origin of an exceptionally Cr-rich
716 kyanite-bearing clinopyroxenite xenolith from Mbuji-Mayi kimberlite (DRC) European
717 Journal of Mineralogy, 23, 257-268.

718 Rapp, R.P., Watson, E.B., and Miller, C.F. (1991) Partial melting of amphibolite/eclogite and
719 the origin of Archean trondhjemites and tonalites. Precambrian Research, 51, 1-25.
720 Reid, A.M., Brown, R.W., Dawson, J.B., Whitfield, G.G., and Siebert, J.C. (1976) Garnet and
721 Pyroxene compositions in some diamondiferous eclogites. Contributions to Mineralogy
722 and Petrology, 58, 203-220.
723 Ringwood, A.E., and Major, A. (1971) Synthesis of majorite and other high pressure garnets
724 and perovskites. Earth and Planetary Science Letters, 12, 411-441.
725 Rossi, G. (1988) A review of the crystal-chemistry of clinopyroxenes in eclogites and other
726 high-pressure rocks. In D.C. Smith, Ed., Eclogites and Eclogite-facies Rocks,
727 Developments in Petrology 12, Elsevier, 237-270.
728 Ruiz-Cruz, M.D., and Sanz de Galdeano, C. (2013) Coesite and diamond inclusions,
729 exsolution microstructures and chemical patterns in ultrahigh pressure garnet from Ceuta
730 (Northern Rif, Spain) Lithos, 177, 184-206.
731 Schmädicke, E., Okrusch, M., and Schmidt, W. (1992) Eclogite-facies rocks in the Saxonian
732 Erzgebirge, Germany: high pressure metamorphism under contrasting *P-T* conditions.
733 Contributions to Mineralogy and Petrology, 110, 226-241.
734 Sen, C., and Dunn, T. (1994) Dehydration melting of a basaltic composition amphibolite at
735 1.5 and 2.0 GPa: implications for the origin of adakites. Contributions to Mineralogy and
736 Petrology, 117, 394-409.
737 Smith, C.B., Bulanova, G.P., Kohn, S.C., Milledge, H.J., Hall, A.E., Griffin, B.J. and Pearson,
738 D.G. (2009) Nature and genesis of Kalimantan diamonds. Lithos, 112S, 822-832
739 Smyth, J.R., and Hatton, C.J. (1977) A coesite-sanidine grospydite from the Roberts Victor
740 kimberlite. Earth and Planetary Science Letters, 34, 284-290.
741 Song, S., Yang, J., Liou, J.G., Wu, C., Shi, R., and Xu, Z. (2003) Petrology, geochemistry and
742 isotopic ages of eclogites from the Dulan UHPM terrane, the North Qaidam, NW China.
743 Lithos, 70, 195-211.

744 Spandler, C., Yaxley, G., Green, D.H., and Rosenthal, A. (2008) Phase relations and melting
745 of anhydrous K-bearing eclogite from 1200-1600°C and 3 to 5 GPa. Journal of Petrology,
746 49, 771-795.
747 Spear, F.S., and Pyle, J.M. (2004) Apatite, monazite, and xenotime in metamorphic rocks. In
748 M.J. Kohn, J. Rakovan, and J.M. Hughes, Eds., Phosphates-Geochemical, Geobiological,
749 and Materials Importance; Reviews in Mineralogy and Geochemistry, vol. 48,
750 Mineralogical Society of America, Geochemical Society; Washington, D.C., 293-335.
751 Stachel, T., Harris, J:W., and Brey, G.P. (1998) REE patterns of peridotitic and eclogitic
752 inclusions in diamonds from Mwadui (Tanzania). In J.J. Gurney, J.L. Gurney, M.D.
753 Pascoe, and S.H. Richardson, Eds., Proceedings of the VIIth International Kimberlite
754 Conference; Red Roof Design cc, Cape Town, South Africa, pp. 829-835.
755 Stachel, T., Aulbach, S., Brey, G.P., Harris, J.W., Loest, I., Tappert, R., and Viljoen, K.S.
756 (2004) The trace element composition of silicate inclusions in diamonds: a review.
757 Lithos, 77, 1-19.
758 Sugiyama, K., and Tokonami, M. (1987) Structure and crystal chemistry of a dense
759 polymorph of tricalcium phosphate $Ca_3(PO_4)_2$: a host to accommodate large lithophile
760 elements in the Earth's mantle. Physics and Chemistry of Minerals, 15, 125-130.
761 Svensen, H., Jamtveit, B., Banks, D.A. and Austrheim, H. (2001) Halogen contents of
762 eclogite facies fluids and minerals: Caledonides, western Norway. Journal of
763 Metamorphic Geology, 19, 165-178.
764 Tappert, R., Stachel, T., Harris, J:W., Muehlenbachs, K., Ludwig, T., and Brey, G.P. (2005)
765 Diamonds from Jagersfontein (South Africa): messengers from the sublithospheric
766 mantle. Contributions to Mineralogy and Petrology, 150, 505-522.
767 Taylor, L.A., Anand, M., Promprated, P., Floss, C., and Sobolev, N.V. (2003) The
768 significance of mineral inclusions in large diamonds from Yakutia, Russia. American
769 Mineralogist, 88, 912-920.

Thilo, E. (1941) Über die Isotypie zwischen Phosphaten der allgemeinen Zusamensetzung $(Me_1)_3(Me_2)_2[PO_4]_3$ und den Silikaten der Granatgruppe. Naturwissenschaften, 29, 239.

Thompson, R.N. (1975) Is upper mantle phosphorus contained in sodic garnet ? Earth and Planetary Science Letters, 26, 417-424.

Tong, L., Jahn, B.-M., Iizuka, Y., and Xu, Z. (2007) Assemblages and textural evolution of UHP eclogites from the Chinese Continental Scientific Drilling Main Hole. International Geology Review, 49, 73-89.

Vrána, S., and Fryda, J. (2003) Ultrahigh-pressure grossular-rich garnetite from the Moldanubian Zone, Czech Republic. European Journal of Mineralogy, 15, 43-54.

Watson, E.B. (1979) Apatite saturation in basic to intermediate magmas. Geophysical Research Letters, 6, 937-940.

Watson, E.B., and Capobianco, C.J. (1981) Phosphorus and rare earth elements in felsic magmas: an assessment of the role of apatite. Geochimica et Cosmochimica Acta, 45, 2349-2358.

Watson, E.B., and Cherniak, D.J. (2014) Diffusion of phosphorus in olivine. Goldschmidt Abstracts, 2014, 2665

Watt, G.R. (1995) High-thorium monazite-(Ce) formed during disequilibrium melting of metapelites under granulite-facies conditions. Mineralogical Magazine, 59, 735-743.

Wieczorek, A., and Beran, A. (2003) OH defects in high-pressure kyanite. EGS-AGU-EUG Joint Assembly, abstract #6670;

Wieczorek, A., Libowitzky, E., and Beran, A. (2004) A model for the OH defect incorporation in kyanite based on polarized IR spectroscopic investigations. Schweizerische Mineralogische und Petrographische Mitteilungen, 84, 333-343.

Xia, Q.-K., Sheng, Y.-M., Yang, X.-Z., and Yu, H.-M. (2005) Heterogeneity of water in garnets from UHP eclogites, eastern Dabieshan, China. Chemical Geology, 224, 237-246.

795 Xie, X., Minitti, M. E., Chen, M., Mao, H-K, Wang, D., Shu, J., and Fei, Y. (2003) Tuite, γ-
796 $Ca_3(PO_4)_2$: a new mineral from the Suizhou L6 chondrite. European Journal of
797 Mineralogy, 15, 1001-1005.
798 Yang, J. and Liu, L. (2004) Coupled isomorphic substitution and exsolution of pyroxene,
799 rutile, apatite and quartz in supersilicic garnet. Chinese Science Bulletin, 49, 70-75.
800 Ye, K., Liu, J.-B., Cong, B.-L., Ye, D.-N., Xu, P., Omori, S., and Maruyama, S. (2002)
801 Ultrahigh-pressure (UHP) low-Al titanites from carbonate-bearing rocks in Dabieshan-
802 Sulu UHP terrane, eastern China. American Mineralogist, 87, 875-881.
803 Zeming, Z., Zhiqin, X., and Huifen, X. (2000) Petrology of ultrahigh-pressure eclogites from
804 the ZK703 drillhole in the Donghai, eastern China. Lithos, 52, 35-50.
805 Zhang, R.Y., Liou, J.G., Ernst, W.G., Coleman, R.G., Sobolev, N.V., and Shatsky, V.S.
806 (1997) Metamorphic evolution of diamond-bearing and associated rocks from the
807 Kokchetav Massif, northern Kazakhstan. Journal of Metamorphic Geology, 15, 479-496.
808 Zhang, R.Y., Zhai, S.M., Fei, Y.W., and Liou, J.G. (2003a) Titanium solubility in coexisting
809 garnet and clinopyroxene at very high pressure: the significance of exsolved rutile in
810 garnet. Earth and Planetary Science Letters, 216, 591-601.
811 Zhang, R.Y., Liou, J.G., Zheng, Y.F., and Fu, B. (2003b) Transition of UHP eclogites to
812 gneissic rocks of low-amphibolite facies during exhumation: evidence from the Dabie
813 terrane, central China. Lithos, 70, 269-291.
814 Zhang, G., Ellis, D.J., Christy, A.G., Zhang, L., Niu, Y., and Song, S. (2009) UH*P*
815 metamorphic evolution of coesite-bearing eclogites from the Yuka terrane, North Qaidam
816 UH*P*M belt, NW China. European Journal of Mineralogy, 21, 1287-1300.
817 Zheng, Y.-F., Xia, Q.-X., Chen, R.-X., and Gao, X.-Y. (2011). Partial melting, fluid
818 supercriticality and element mobility in ultrahigh-pressure metamorphic rocks during
819 continental collision. Earth-Science Reviews, 107, 342-374.

Zhitova, L.M., Sharygin, V.V., and Kamenetsky, V.S. (2013) Phosphorus-bearing pyroxenes in flood basalts with native iron, Khungtukun, Polar Siberia, Russia. DOI: 10.1180/minmag.2013.077.5.26

Figure Captions

Figure 1

BSE photomicrographs of experimental charges. **(a)** run MA65: compositionally homogeneous Na-P-rich garnet with strongly variable grain size from ≤1-2 to ~30 μm and traces of kyanite used for preparation of bulk-I. **(b)** run JKI-116: garnet + clinopyroxene + quartz + rutile + apatite formed by recrystallization of bulk-I. Kyanite is thought to be inherited from run MA65. **(c)** run JKI-118: newly formed apatite intergrown with garnet. **(d)** run JKI-149: apatite inclusions in clinopyroxene present as isolated grains and as clusters of grains. **(e)** run JKI-147: large euhedral interstitial apatite with clinopyroxene inclusion. **(f)** run JKI-133: small melt pool formed within apatite-free garnet + clinopyroxene + orthopyroxene + rutile matrix just above the solidus. **(g)** run JKI-141: tiny apatites coexisting with clinopyroxene + kyanite + quartz + rutile + vapour-saturated melt stable in bulk-II. **(h)** run JKI-141: coexisting Na-rich (cpx-I) and Na-poor (cpx-II) clinopyroxenes. Abbreviations: grt garnet; cpx clinopyroxene; opx orthopyroxene; qtz quartz; rt rutile; ap apatite; ky kyanite;

Figure 2

Frequency and size distribution of apatites formed by breakdown of Na-P-rich garnet.

Figure 3

(a) BSE photomicrograph of garnets coexisting with pyroxenes and rutile from run JKI-118. **(b)-(d)** element distribution maps for P, Ti, and Na showing compositional zoning of the

garnets with P-Na-depletion and Ti-enrichment in the rims. White stippled lines mark approximate garnet grain boundaries. Note apatite-inclusion in garnet (lowermost portion of BSE image).

Figure 4

(a) BSE photomicrograph of zoned garnet from run JKI-147 with Na-P-rich core (area within white stippled line) and Na-P-depleted and Ti-rich rim. **(b)** compositional profile across zoned garnet. Error bars are 2σ errors for individual analyses. **(c)** Na vs. P (apfu) for garnet cores and rims indicating $^{[8]}Na^{[4]}P^{[8]}M^{2+}_{-1}{}^{[4]}Si_{-1}$ exchange.

Figure 5

Averaged P contents of clino- and orthopyroxene from the experiments using bulk-I.

Figure 6

(a) BSE photomicrograph and **(b)** P distribution map for kyanite and coexisting phases from run JKI-116. **(c)** BSE photomicrograph and **(d)-(f)** element distribution maps for P, Mg and Ti for kyanite from run JKI-141.

Figure 7

Schematic Schreinemakers arrangement in a *P-T* section of possible apatite-forming reactions involving breakdown of $Na_3Al_2(PO_4)_3$-phase component in garnet in the system P_2O_5-SiO_2-Al_2O_3-MgO-CaO-Na_2O-H_2O, which is consistent with a positive slope for the reaction grs + en = prp + di. Reactions were balanced using the REACTION program by Finger and Burt (1972). For abbreviations see text.

872 **TABLE 1.** Compositions of the starting materials
873

	(1) model eclogite	(2) Na-P-rich garnet	(3) bulk-I	(4) bulk-II
SiO_2 [wt%]	55.4	43.3(3)	53.8	61.0
TiO_2	1.4	-----	1.2	0.7
Al_2O_3	9.3	24.6(1)	10.6	14.4
MgO	18.9	24.8(3)	19.9	1.6
CaO	13.8	6.3(4)	13.0	4.8
Na_2O	1.3	0.3(0)	1.2	1.1
P_2O_5	-----	0.7(1)	0.1	0.7
H_2O	-----	-----	0.3	15.6[a]
∑	100.0	100.0	100.0	100.0

874 (1) model eclogite (Konzett and Frost 2009)
875 (2) average composition (n=8) of Na-P-rich garnet used for bulk-I
876 (3) bulk-I (model eclogite + 10% Na-P-rich garnet + 1% $Mg(OH)_2$)
877 (4) bulk-II (composition of melt generated from bulk-I at 2 GPa/1000°C)
878 [a]amount of water estimated from EMPA analytical totals and added
879 with a micro-syringe.
880

881

882

883

884 **TABLE 2.** Summary of experimental run conditions and run products
885

run No.	starting mat.	P[GPa]	T[°C]	duration	phases observed	ap/UA[a]	∑ap-areas/UA[b]
MA65	Na-P-rich grt	7.0	1200	134h15min	grt+ky		
JKI-116	bulk-I	2.0	850	434h13min	grt+cpx+qtz+rt+**ap (**+ky+mgs)	2.7	22.7
JKI-118	bulk-I	2.0	950	504h20min	grt+cpx+opx+qtz+rt+**ap**	0.6	18.6
JKI-147	bulk-I	2.0	975	501h34min	grt+cpx+opx+qtz+rt+**ap**	0.6	18.1
JKI-133	bulk-I	2.0	1000	462h29min	grt+cpx+opx+rt+**melt**		
JKI-149	bulk-I	2.0	1000→950	484h34min	grt+cpx+opx+qtz+rt+**ap**	1.8	13.5
JKI-141	bulk-II	2.0	800	310h47min	cpx+qtz+ky+rt+zoi+**ap+melt**		

886 [a]Average number of apatites counted per unit area of 10000 μm^2. [b]Total area of apatite grains per unit area with areas of apatite grains
887 calculated as outlined in the text. Abbreviations: grt garnet, cpx clinopyoxene, opx orthopyroxene, qtz quartz, ky kyanite, rt rutile, mgs
888 magnesite, ap apatite, zoi zoisite.
889
890

891

892

893

894

TABLE 3. Averaged and representative analyses of garnet, kyanite, and quenched melt

run # (bulk)	JKI-118 (I)		JKI-147 (I)			JKI-116 (I)	JKI-41 (II)	JKI-133 (I)	JKI-141 (II)
P[GPa]/T[°C]	2.0/950		2.0/975			2.0/850	2.0/800	2.0/1000	2.0/800
phase	grt (core)	grt (rim)	grt (core)	grt (rim-1)	grt (rim-2)	ky	ky	melt	melt
# of analyses						4	5	4	6
SiO_2	43.82	44.31	43.80	43.90	43.92	37.71(13)	37.33(51)	61.05(49)	65.58(54)
TiO_2	<0.05	0.23	<0.05	0.35	0.37	<0.05	0.46(11)	0.67(04)	0.11(03)
Al_2O_3	24.77	24.69	24.83	25.64	24.92	63.37(21)	61.18(27)	14.45(17)	13.62(14)
MgO	25.68	26.15	25.86	25.28	25.82	0.22(01)	0.56(06)	1.62(09)	0.53(03)
CaO	5.84	5.33	5.61	6.43	6.09	nd	nd	4.79(13)	2.33(12)
Na_2O	0.26	0.08	0.25	0.09	0.05	nd	nd	1.11(37)	5.07(48)
P_2O_5	0.65	0.17	0.60	0.29	0.17	0.17(00)	0.20(04)	0.72(10)	0.07(01)
Cl	nd	nd	nd	nd	nd	nd	nd	0.17(01)[a]	0.34(04)[a]
∑	101.02	100.73	100.95	101.63	100.97	101.47(29)	99.72(38)	84.40(22)	87.30(50)
Si	2.961	2.992	2.960	2.944	2.963	1.002(02)	1.010(11)		
Ti	-------	0.012	-------	0.018	0.019	-------	0.009(02)		
Al	1.973	1.965	1.978	2.027	1.981	1.985(02)	1.951(13)		
Mg	2.585	2.632	2.605	2.527	2.596	0.009(00)	0.022(02)		
Ca	0.423	0.386	0.406	0.462	0.440	-------	-------		
Na	0.034	0.010	0.033	0.012	0.007	-------	-------		
P	0.037	0.010	0.034	0.016	0.010	0.004(00)	0.005(00)		
Cl	-------	-------	-------	-------	-------	-------	-------		
∑	8.014	7.993	8.016	7.988	7.997	3.000(01)	2.998(03)		

garnet and kyanite formulae normalized to 12 and 5 oxygens, respectively; [a]Cl analyzed using averaged melt composition for matrix correction.

TABLE 4. Averaged and representative analyses of pyroxenes

run # (bulk)	JKI-116 (I)	JKI-118 (I)		JKI-147 (I)		JKI-149 (I)	JKI-133 (I)		JKI-141 (II)	
P[GPa]/T[°C]	2.0/850	2.0/950		2.0/975		2.0/1000 →950	2.0/1000		2.0/800	
phase	cpx	cpx	opx	cpx	opx	cpx	cpx	opx	cpx-I	cpx-II
# of analyses	8	10	3	6	2	4	10	1	6	2
SiO_2	54.67(48)	53.52(43)	57.54(43)	54.30(36)	57.83(10)	53.06(32)	54.39(43)	58.38	54.85(63)	55.49(57)
TiO_2	0.35(07)	0.45(06)	0.14(04)	0.44(07)	0.11(01)	0.60(06)	0.52(07)	0.11	0.83(15)	0.11(03)
Al_2O_3	7.83(70)	7.89(67)	5.10(133)	6.67(81)	4.39(52)	8.33(81)	7.85(67)	4.47	12.92(91)	5.16(59)
MgO	15.71(47)	16.24(40)	37.58(65)	16.73(42)	37.14(70)	15.74(50)	16.18(30)	39.17	10.42(49)	15.42(11)
CaO	21.11(52)	21.20(36)	0.59(07)	21.55(42)	0.58(00)	20.03(33)	20.50(39)	0.62	16.21(84)	21.67(32)
Na_2O	2.13(13)	1.79(10)	0.12(04)	1.41(13)	0.10(06)	1.77(03)	1.96(19)	0.07	5.12(42)	2.06(19)
∑	101.79(76)	102.09(49)	101.06(60)	101.10(28)	100.14(03)	99.52(48)	101.39(92)	102.82	100.35(73)	99.89(96)
Si	1.909(11)	1.898(12)	1.907(25)	1.911(12)	1.931(02)	1.891(09)	1.904(12)	1.904	1.917(07)	1.976(02)
Ti	0.009(02)	0.012(02)	0.003(01)	0.012(02)	0.003(00)	0.016(02)	0.014(02)	0.003	0.022(04)	0.003(01)
Al	0.322(29)	0.324(28)	0.199(51)	0.277(33)	0.173(20)	0.350(34)	0.324(26)	0.172	0.532(35)	0.217(22)
Mg	0.818(22)	0.843(20)	1.856(37)	0.878(23)	1.849(36)	0.836(27)	0.844(14)	1.904	0.543(27)	0.819(15)
Ca	0.790(18)	0.791(14)	0.021(02)	0.813(17)	0.021(00)	0.765(11)	0.769(19)	0.022	0.607(34)	0.827(22)
Na	0.144(09)	0.121(07)	0.008(03)	0.096(09)	0.006(04)	0.122(02)	0.133(12)	0.004	0.347(26)	0.142(12)
∑	3.992(07)	3.989(06)	3.994(07)	3.987(05)	3.983(10)	3.979(09)	3.987(03)	4.009	3.968(05)	3.983(04)
µg/g P	262±81 [7]	341±47 [9]	237±37 [3]	159±76 [7]		190±44 [4]	178±32 [7]	59±16	148±21 [5]	
CaEs (mol%)	1.5	2.3		2.7		4.1	2.6		6.3	3.3
Cats	9.1	10.2		8.9		10.9	9.7		8.3	2.4
Jd	12.6	9.7		7.2		9.0	10.5		30.3	13.6
Di	69.2	67.8		71.1		63.5	66.0		49.3	78.7
En	5.9	7.7		7.8		9.2	8.5		1.4	1.5
NaTi-px	1.8	2.4		2.4		3.2	2.8		4.4	0.6

pyroxene analyses normalized to 6 oxygens; numbers in brackets are standard deviations of averaged analyses; numbers in square brackets refer to number of clinopyroxenes analyzed for P; for single orthopyroxene analyses, errors given are 2σ-errors for the individual analysis; abbreviations: CaEs Calcium Eskola pyroxene; Cats Calcium Tschermak's pyroxene; NaTi-px Na-Ti-pyroxene

933 **TABLE 5.** Representative analyses of apatite
934

run # (bulk)	JKI-116 (I)	JKI-18 (I)	JKI-147 (I)
P[GPa]/T[°C]	2.0/850	2.0/950	2.0/975
P_2O_5	42.29	42.19	41.73
SiO_2	0.12	0.29	0.37
CaO	54.71	53.36	54.54
MgO	0.66	0.93	1.05
Na_2O	<0.05	0.15	<0.05
Cl	2.64	3.62	0.77
H_2O[a]	1.11	0.86	1.59
∑	101.54	101.40	100.09
-Cl=O	0.60	0.82	0.17
∑	100.94	100.58	99.92
P	2.997	3.005	2.962
Si	0.010	0.024	0.031
Ca	4.906	4.810	4.899
Mg	0.082	0.117	0.131
Na	-------	0.024	-------
∑	7.995	7.981	8.030
Cl	0.374	0.516	0.109
OH	0.625	0.483	0.889

935 apatite analyses normalized to 13 (O, OH, F, Cl)
936 [a]wt% H_2O calculated based on stoichiometry.
937
938
939
940
941
942
943
944
945
946
947
948
949
950
951
952

TABLE 6. Modal amounts of apatite potentially formed by release of P from silicate phases as a function of the eclogite bulk phosphorus content

bulk P_2O_5 content (wt%)	0.10	0.20	0.25
wt% P_2O_5 stored in grt	0.08	0.08	0.08
wt% P_2O_5 stored in cpx	0.02	0.02	0.02
wt% excess P_2O_5	-----	0.10	0.15
% modal ap equivalent to P in grt	0.18	0.18	0.18
% modal ap equivalent to P in cpx	0.05	0.05	0.05
% modal ap equivalent to excess P_2O_5	-----	0.24	0.36
proportion (%) of ap formed from P in grt	78	38	31
proportion (%) of ap formed from P in cpx	22	11	9
proportion (%) of excess ap	---	51	61

model calculations are based on the following assumptions:
(1) *P* at peak of metamorphism: 4-6 GPa
(2) P_2O_5-solubility in grt and cpx: 0.25 wt% and 0.039 wt% (=170 µg/g P) (cf. Konzett and Frost (2009)
(3) modal proportion of phases: 30% grt + 60% cpx + 10% phases with negligible P
(4) 42.4 wt% P_2O_5 in ap

Figure 1

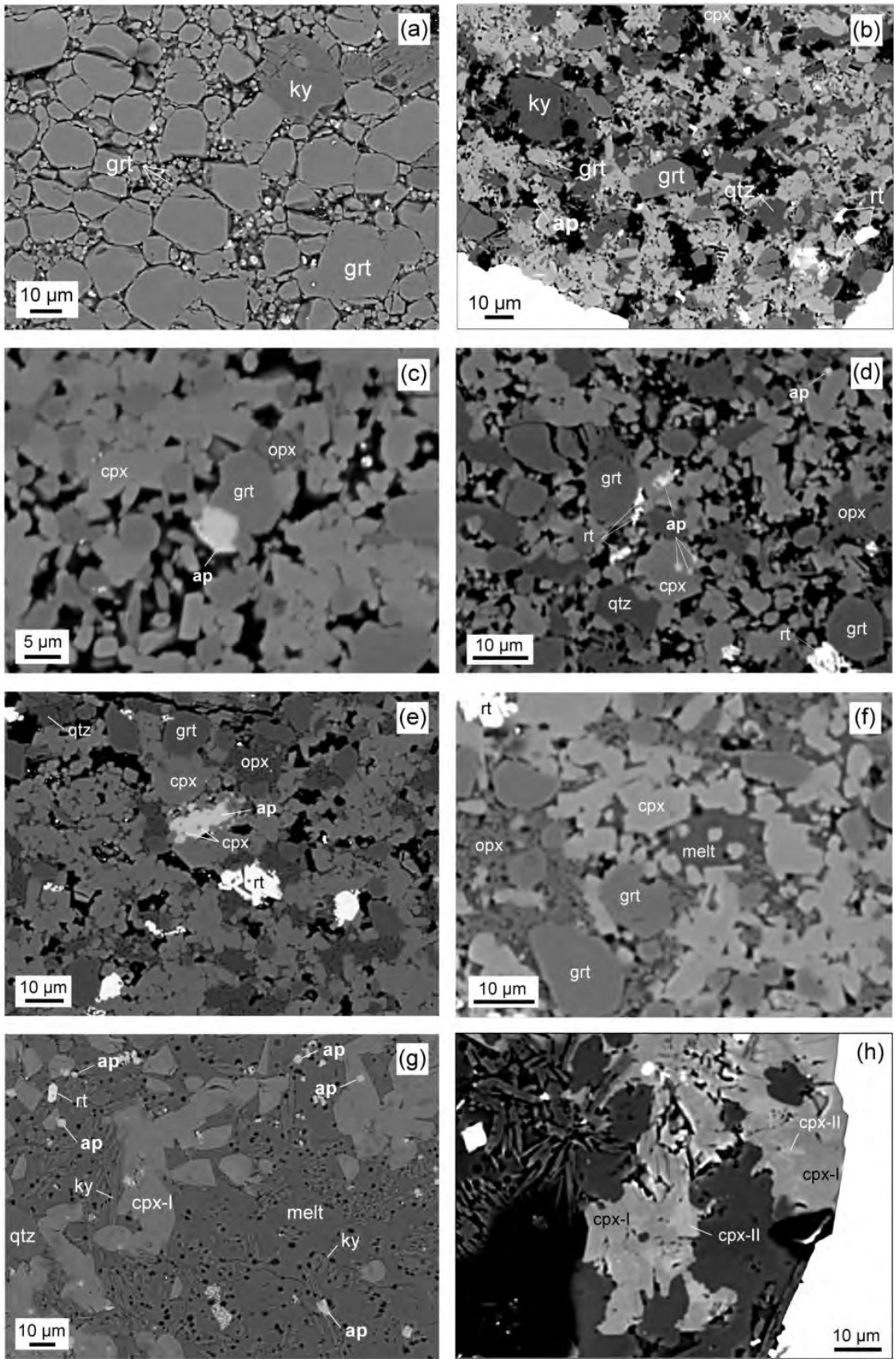
(a)
ky
grt
grt
10 µm
(b)
cpx
ky
grt
grt
qtz
rt
ap
10 µm
(c)
opx
cpx
grt
ap
5 µm
(d)
ap
grt
opx
rt
ap
cpx
qtz
rt
grt
10 µm
(e)
qtz
grt
opx
cpx
ap
cpx
rt
10 µm
(f)
rt
cpx
opx
melt
grt
grt
10 µm
(g)
ap
ap
ap
rt
ap
ap
ky
cpx-I
melt
qtz
ky
ap
10 µm
(h)
cpx-II
cpx-I
cpx-I
cpx-II
10 µm

Figure 2

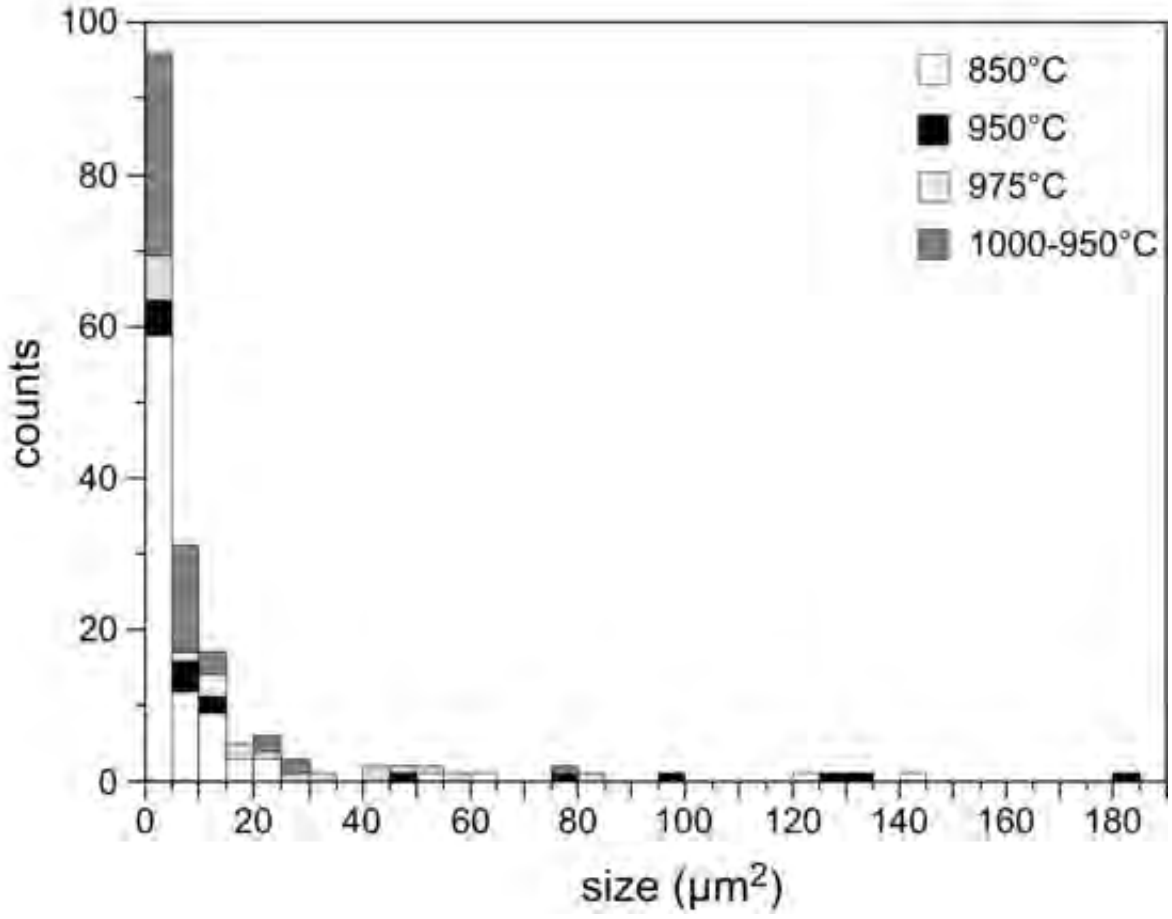
100
80
60
40
20
0
counts
0
20
40
60
80
100
120
140
160
180
size (μm²)
850°C
950°C
975°C
1000-950°C

Figure 3

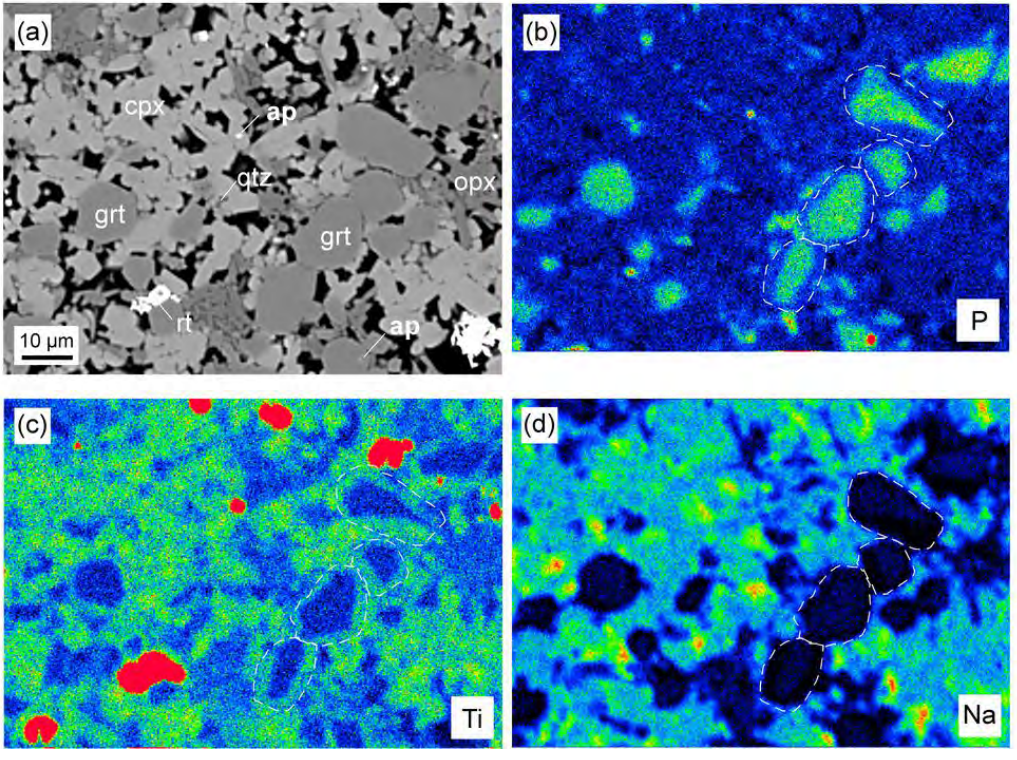

Figure 4

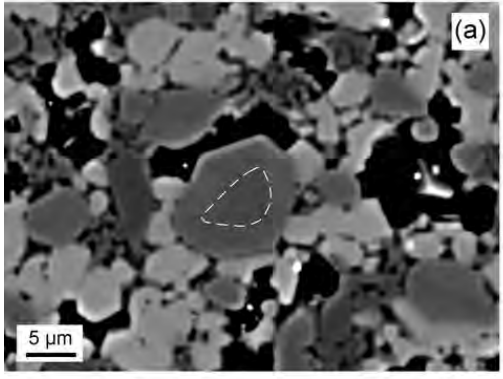
(a)
5 µm

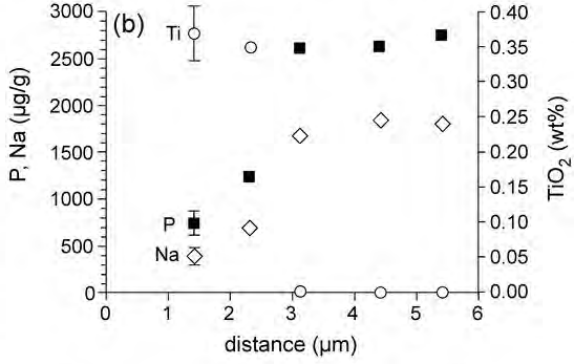
(b)
Ti
P
Na
P, Na (µg/g)
TiO2 (wt%)
distance (µm)
3000
2500
2000
1500
1000
500
0
0.40
0.35
0.30
0.25
0.20
0.15
0.10
0.05
0.00
0
1
2
3
4
5
6

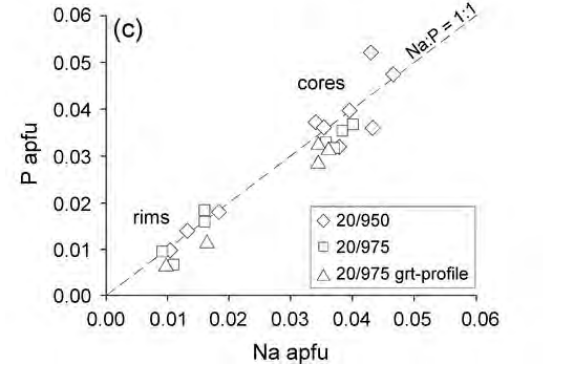
(c)
Na:P = 1:1
cores
rims
20/950
20/975
20/975 grt-profile
P apfu
Na apfu
0.06
0.05
0.04
0.03
0.02
0.01
0.00
0.00
0.01
0.02
0.03
0.04
0.05
0.06

Figure 5

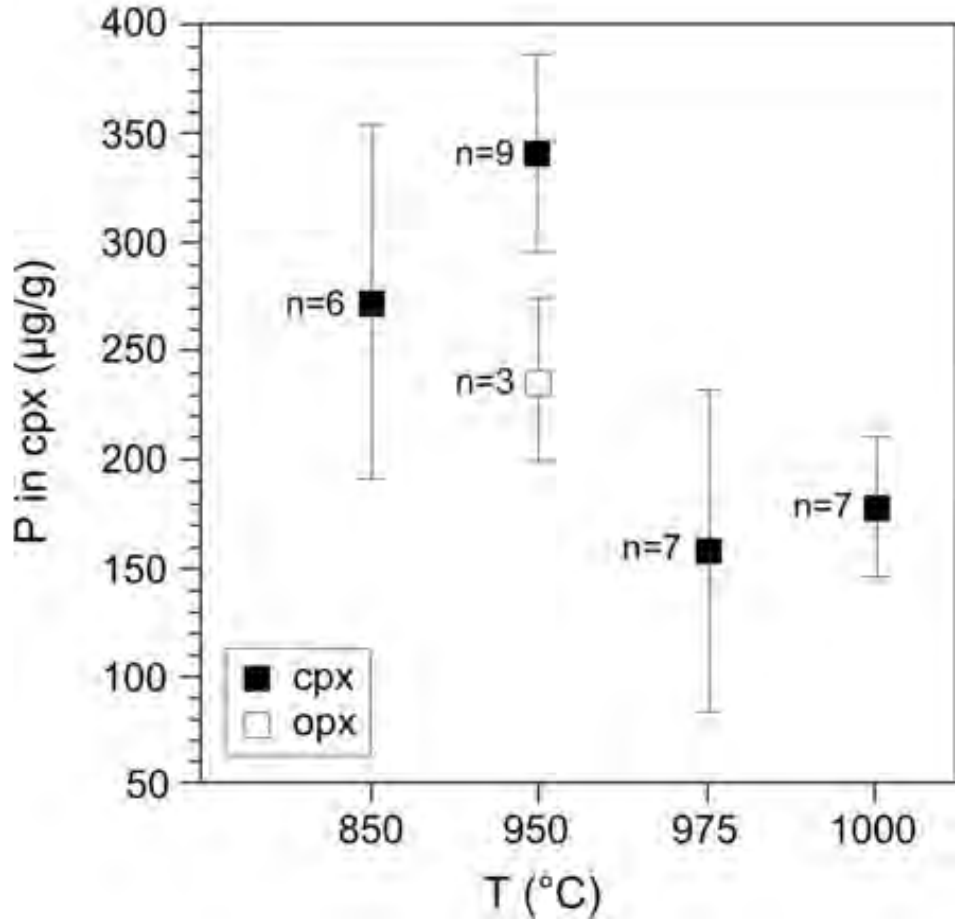
400
350
300
250
200
150
100
50
P in cpx (µg/g)
n=9
n=6
n=3
n=7
n=7
cpx
opx
850
950
975
1000
T (°C)

Figure 6

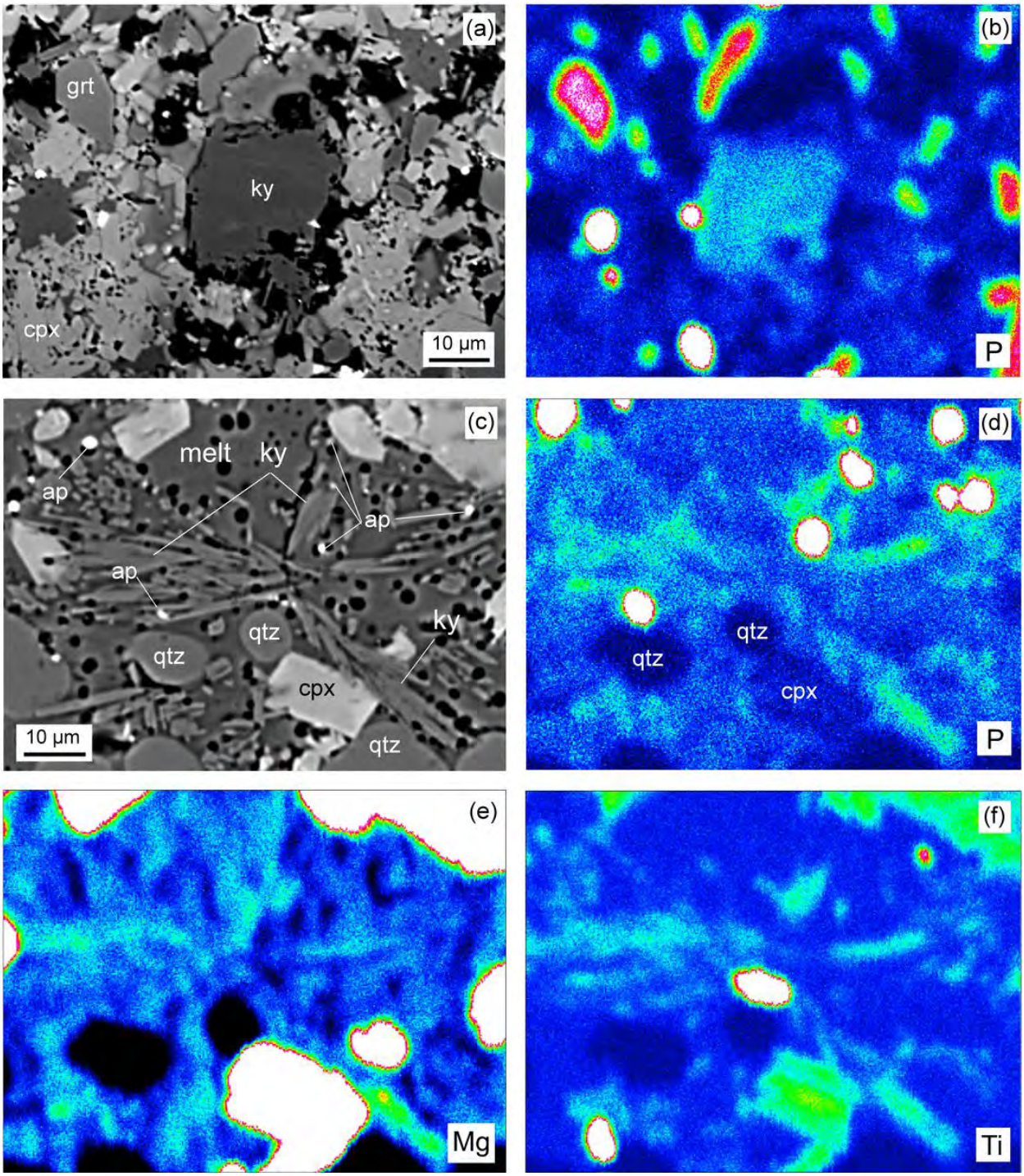
(a)
grt
ky
cpx
10 μm
(b)
P
(c)
melt
ky
ap
ap
ap
qtz
qtz
ky
cpx
qtz
10 μm
(d)
qtz
qtz
cpx
P
(e)
Mg
(f)
Ti

Figure 7

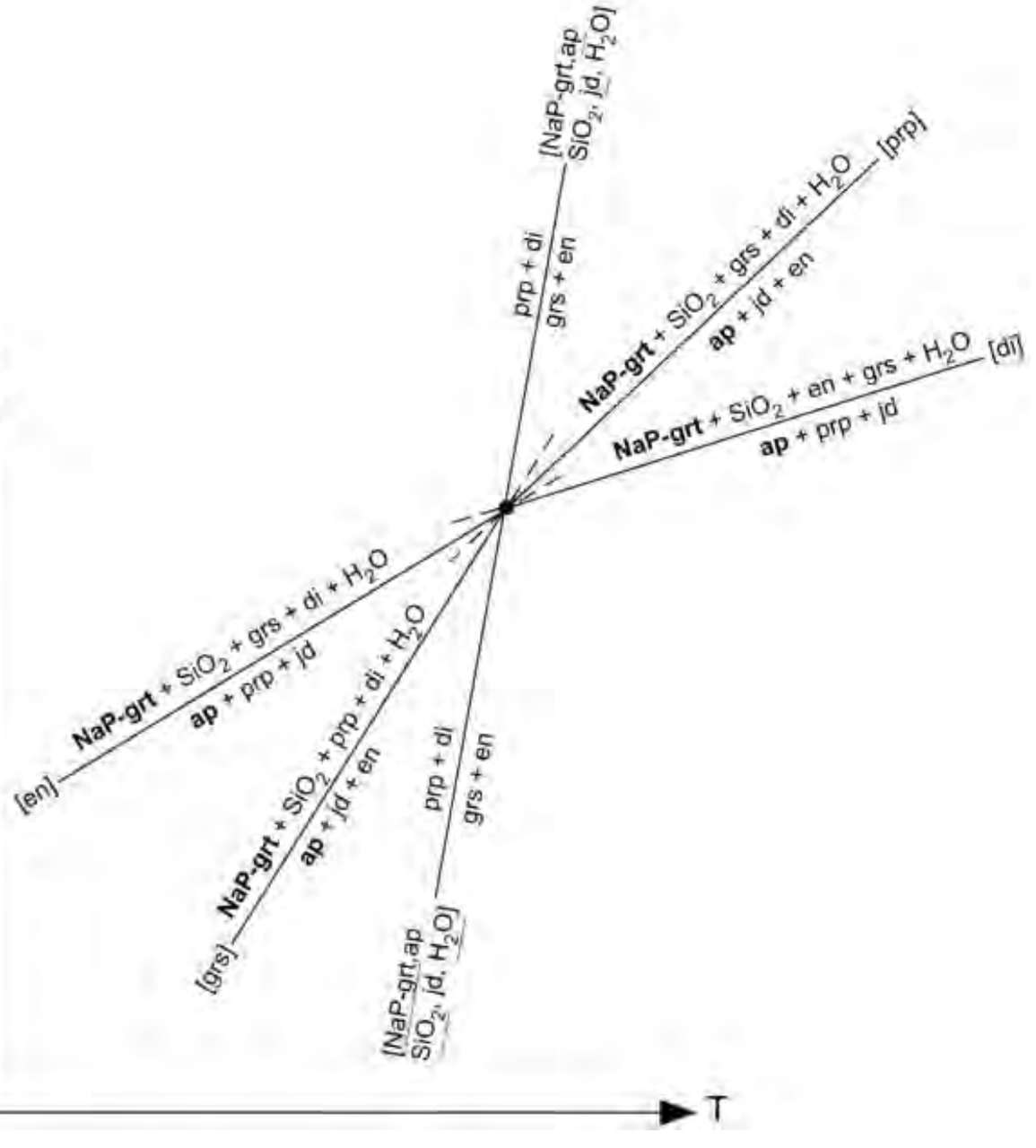
P
T
[NaP-grt,ap
SiO2, jd, H2O]
prp + di
grs + en
NaP-grt + SiO2 + grs + di + H2O
ap + jd + en
[prp]
NaP-grt + SiO2 + en + grs + H2O
ap + prp + jd
[di]
[en]
NaP-grt + SiO2 + grs + di + H2O
ap + prp + jd
[grs]
NaP-grt + SiO2 + prp + di + H2O
ap + jd + en
prp + di
grs + en
[NaP-grt,ap
SiO2, jd, H2O]